

# Do Two Temperature Debris Disks Have Multiple Belts?

G. M. Kennedy\*, M. C. Wyatt

*Institute of Astronomy, University of Cambridge, Madingley Road, Cambridge CB3 0HA, UK*

21 September 2018

## ABSTRACT

We present a study of debris disks whose spectra are well modelled by dust emission at two different temperatures. These disks are typically assumed to be a sign of multiple belts, which in only a few cases have been confirmed via high resolution observations. We first compile a sample of two-temperature disks to derive their properties, summarised by the ratios of the warm and cool component temperatures and fractional luminosities. The ratio of warm to cool temperatures is constant in the range 2-4, and the temperatures of both warm and cool components increases with stellar mass. We then explore whether this emission can arise from dust in a single narrow belt, with the range of temperatures arising from the size variation of grain temperatures. This model can produce two-temperature spectra for Sun-like stars, but is not supported where it can be tested by observed disk sizes and far-IR/mm spectral slopes. Therefore, while some two-temperature disks arise from single belts, it is probable that most have multiple spatial components. These disks are plausibly similar to the outer Solar System’s configuration of Asteroid and Edgeworth-Kuiper belts separated by giant planets. Alternatively, the inner component could arise from inward scattering of material from the outer belt, again due to intervening planets. In either case, we suggest that the ratio of warm/cool component temperatures is indicative of the scale of outer planetary systems, which typically span a factor of about ten in radius.

**Key words:** star: circumstellar matter — infrared: stars

## 1 INTRODUCTION

Debris disks are a sign of successful planetesimal formation. The radial structure of most planetesimal belts is unknown; they may lie in multiple rings analogous to the Asteroid and Edgeworth-Kuiper belts, but may also be significantly extended in a way similar to gaseous protoplanetary disks (e.g. Kalas et al. 2005; Su et al. 2009; Wyatt et al. 2012). Because they are generally detected by excess emission above the photospheric level at infra-red (IR) wavelengths (e.g. Aumann et al. 1984), and with high resolution imaging detections being relatively rare, discerning radial structure is in general difficult. The major difficulty is that the equilibrium temperature of a dust grain depends on both distance from the star and the size and optical properties of that dust grain. Thus, the radius of an unresolved debris disk cannot be unambiguously determined from the temperature of the observed emission, as the temperature is degenerate with the sizes of grains in the disk.

Infra-red excess detections are generally well approximated by a single blackbody. This property is in part due to the emission properties of circumstellar dust, but also due to a lack of a high disk signal to noise ratio over a wide range of

wavelengths. However, an increasing number of more complex systems are being discovered with the help of mid-IR spectra, which when combined with far-IR photometry show emission at more than one temperature, and therefore may be indicative of dust that resides at a range of stellocentric distances (e.g. Backman et al. 2009; Chen et al. 2009; Morales et al. 2009; Ballering et al. 2013). Such disks can be modelled in different ways, but a promising approach is simply to add a second blackbody component (e.g. Chen et al. 2009; Morales et al. 2011; Chen et al. 2014; Ballering et al. 2013). These “two-temperature” disks may be analogous to the Solar System, because a possible interpretation of two temperatures is an origin in dust emission from two distinct radial locations. Again by analogy with the Solar System, a further question is then whether the intervening region between the two belts contains planets, and if so, whether dynamical clearing by these planets is the reason for two-belt structure. Circumstantial evidence for such a picture is given by systems with planets that reside between two dust components, such as HR 8799 and HD 95086 (Marois et al. 2008; Reidemeister et al. 2009; Rameau et al. 2013; Moór et al. 2013).

An alternative interpretation is that the two belts may be linked by intervening planets, with material from an outer belt delivered to replenish the inner belt (e.g. Nesvorný et al.

\* Email: gkennedy@ast.cam.ac.uk

2010; Bonsor & Wyatt 2012). From a study of many disks, Morales et al. (2011) concluded that the warmer of the two temperatures was typically  $\sim 190\text{K}$ , regardless of whether the host star was Sun-like or an A-type. They argue that the common warm dust temperatures may be a signature of sublimating comets passed in from outer regions, or asteroid belt analogues formed just interior to the system’s “snow line”.

Yet a third interpretation, where the two components are linked by grain dynamics (as opposed to planetesimal dynamics), relies on Poynting-Robertson (PR) drag (e.g. Burns et al. 1979). In this case grains “leak” inwards from the planetesimal belt, but are depleted by collisions with other grains as they drift inwards (Wyatt 2005; van Lieshout et al. 2014). A steady state is reached that balances the rates at which particles fill the region interior to the parent belt and are removed by collisions. This process does not lead to very large levels of dust inside the parent belt, but recent work coupled with increased mid-IR sensitivity has led to the conclusion that PR drag makes an important contribution in some systems (Reidemeister et al. 2011; Löhne et al. 2012; Schüppler et al. 2014).

Clearly, such interpretations present interesting possibilities for discerning planetary system structure and the dynamics of such systems. The origin and evolution of the putative warm components is of particular interest, since dust in the habitable zone may impact a future space mission to directly image and characterise exo-Earths (e.g. Beichman et al. 2006; Roberge et al. 2012). For example, Kennedy & Wyatt (2013) show how the known population of warm bright debris disks detected at  $12\mu\text{m}$  can be extrapolated to fainter levels by assuming that those disks are independent of any outer cool belts (i.e. evolve in situ). If the warm belts are replenished by comet delivery from elsewhere, such an extrapolation cannot be made.

Taking a step back however, the interpretation of two-temperature debris disks as physically extended or multiple discrete structures has only been tested in a few cases because it requires dedicated high-resolution observations. For example,  $\eta$  Tel shows what clearly appears to be a two-temperature disk spectrum (Fig. 1), but to confirm that the disk indeed comprises two distinct components has required high resolution mid-IR observations (Smith et al. 2009a).

Therefore, our goal here is to consider a third model that could undermine work that assumes that a broad disk spectrum is always the result of extended or multiple disk components; namely that the debris may be confined to a relatively narrow belt and the breadth of the spectrum simply arises due to the absorption and emission properties of the dust (e.g. Matthews et al. 2007). It is well known that grains of different sizes can have different temperatures at a fixed stellocentric distance. It is also known that debris disks comprise not grains of a single size, but a distribution that extends from  $\mu\text{m}$  to at least cm sizes. Therefore, the specific question we wish to address here is whether two-temperature disks necessarily imply multiple dust components, or if their spectra can be reproduced by plausible grain populations residing in a narrow planetesimal belt. Though it is likely an important effect that contributes significantly in some cases, we do not consider PR drag here. We first compile a sample of two-temperature debris disks (sections 2 & 3) and then discuss their properties (section 4). We then consider whether these disks can be modelled as single belts (section 5), and discuss the models and the origin of multiple belts (section 6).

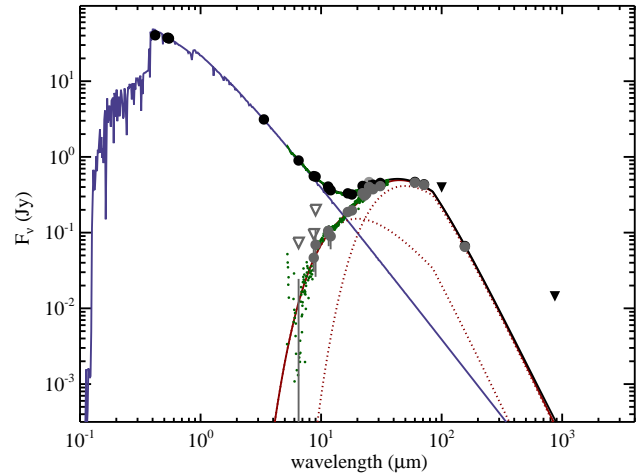


**Figure 1.** SED for  $\eta$  Telescopii. Dots show detections and triangles are upper limits. Black symbols are raw photometry and brown symbols are star-subtracted (i.e. are disk photometry). The maroon line and dots show the observed and star-subtracted IRS spectra. The blue line shows the stellar photosphere model, the red lines the disk emission, and the black line the star+disk emission. The dotted lines are the two temperature components needed to fit the disk spectrum. The disk spectrum is sufficiently broad that a single temperature blackbody is a poor fit, while a model with two components at temperatures of 255 and 100K with  $\lambda_0 = 85\mu\text{m}$  and  $\beta = 1.4$  works well (the SED fitting is described in detail in section 3).

## 2 SAMPLE

This study was initially inspired by the presence of two-temperature disks among targets in the *Herschel* DEBRIS sample. These targets are outlined by Phillips et al. (2010), and comprise the nearest  $\sim 90$  main-sequence stars of A, F, G, K, and M spectral types (i.e.  $\sim 90$  of each type), excluding those near the Galactic plane. Not all DEBRIS sample stars were observed as part of our *Herschel* programme, some being observed by DUNES (Eiroa et al. 2013) and some as part of a guaranteed time programme (Sibthorpe et al. 2010; Vandenbussche et al. 2010; Acke et al. 2012). With only 9 two-temperature sources in DEBRIS (as defined below), we expand the sample with more two-temperature disks observed by *Spitzer* (Werner et al. 2004). These were selected from a large database of stars with *Spitzer* Infra-Red Spectrograph (IRS, Houck et al. 2004) spectra and other mid/far-IR observations, mostly from IRAS and the Multiband Imaging Photometer for *Spitzer* (MIPS, Rieke et al. 2004) but also including *Herschel* and sub-millimetre photometry where available. The resulting sample has 48 robust two-temperature disks around stars with a range of spectral types (see Table A1). IRS spectra are almost always necessary for two temperatures to be detectable, so these observations set which stars are in our sample. Some sources were specifically targeted with IRS based on known excesses (e.g. from IRAS), so the sample for which two-temperature disks can realistically be detected is therefore biased.

Specifically, our sample includes stars from Morales et al. (2009), who selected known debris disks for observation by IRS based on the presence of  $24\mu\text{m}$  excesses. Morales et al. (2011) found that 46% of these showed evidence for two temperatures. The disks in this sample are probably biased towards having two temperatures because the presence of a warm component

adds extra  $24\mu\text{m}$  emission (e.g. Fig. 1). Similarly, some of our stars are from Chen et al. (2006), who observed a large sample of IRAS-discovered disks with  $60\mu\text{m}$  excesses, with IRS. Given that warm components are generally only visible at wavelengths shorter than  $60\mu\text{m}$ , objects observed in this programme are probably not biased towards two temperatures. However, as we demonstrate below, two temperatures are easier to detect when the overall disk fractional luminosity ( $f \equiv L_{\text{disk}}/L_*$ ) is greater, because the excess is detectable at a higher signal to noise ratio (S/N) over a greater range of wavelengths. Thus, while the Chen et al. (2006) sample may not be biased towards disks having two temperatures, they are biased towards detection of two temperatures. These biases are in general unimportant for this study, though need to be considered for the statistics in section 4.4.

For an analysis of a much larger sample of stars observed with IRS see Chen et al. (2014). Our sample is not meant to be complete, but to provide a sufficient number of sources for us to test whether the two-temperature disks arise from single or multiple belts. Our method for deriving the properties of two-temperature disks is different to Chen et al. (2014), though we arrive at the same broad trends.

### 3 SED MODELLING

Because a disk spectrum must be modelled at least once to determine whether multiple temperature components exist, sample selection is closely linked to SED modelling, which we now outline. For all systems, photometry ranging from optical to sub-mm wavelengths is compiled from a wide variety of sources, including all-sky surveys such as Hipparcos (Perryman & ESA 1997; Høg et al. 2000), 2MASS (Cutri et al. 2003), AKARI (Ishihara et al. 2010), WISE (Wright et al. 2010), and IRAS (Moshir et al. 1990). References for far-IR photometry are given in Table A1 and a compiled list of the (sub-)mm photometry is given in Table A2.

Data from the *Spitzer* mission is a crucial component, with IRS spectra needed in almost all cases to reveal two-temperature disks. These are generally obtained from the Cornell CASSIS database (Lebouteiller et al. 2011). However, the CASSIS database only provides extractions for low resolution stare-mode observations, and in some cases only high resolution map-mode data were taken (e.g. HD 39060= $\beta$  Pic). In these cases, or where previously published spectra were readily available (Chen et al. 2006, 2007, 2009; Su et al. 2013) we preferred these over the CASSIS extractions.

The IRS instrument is split into several modules, and the spectral extractions from the different modules must be aligned in relative terms to produce smooth self-consistent spectra. Previous works have generally aligned the modules simply using a handful of data in the region where the spectra overlap (e.g. Lawler et al. 2009; Chen et al. 2014). We took a slightly different approach, fitting the entire spectrum with a function and allowing the absolute values of all but one module (LL1) to vary as part of the fit, thus forcing the spectrum to be smooth across all modules and ensuring that any issues near the edges of each module did not strongly affect the results. For the fitted function, we used the sum of two power laws and one blackbody, the rationale being that the first power law accounts for the stellar Rayleigh-Jeans tail, and that the blackbody and second power law account for excess emission, which may look like either or a

combination of both (e.g. Morales et al. 2009, 2011). We found this method to work well and produce spectra comparable with previous methods.

Once aligned, the IRS spectra are split into 7 photometric “bands”. Because the absolute value of the spectrum will not necessarily agree with other photometry (the absolute level varies at the  $\sim 10\%$  level, e.g. Lawler et al. 2009), the spectrum is normalised so that the shortest band agrees with synthetic photometry of the best fitting stellar photosphere model. The IRS bands are subsequently treated identically to other photometry. Because the quality of the spectral extractions vary, we found it necessary to add a 2% systematic uncertainty to all spectra to avoid spurious excesses. In most cases this uncertainty dominates, so the formal uncertainty is larger than would be expected from looking at the point to point scatter in the spectrum.

Photometry shortward of about  $10\mu\text{m}$  is used to model the stellar photospheric emission. This wavelength is varied from star to star depending on the temperature of the excess, ensuring both the best photospheric fit and that the excess does not affect this fit. For each star the best fitting model from a grid of PHOENIX AMES-Cond models (Brott & Hauschildt 2005) is found by a combination of brute force grids and least squares fitting. For the few stars found to be over 10,000K we use models from Castelli & Kurucz (2003), which span a wider range of effective temperatures. The remaining IR photometry is used to find the best fitting disk model. We first subtracted synthetic photometry of the photosphere model from the observed fluxes to derive disk fluxes, with uncertainties derived from the photosphere and IR observation (including systematic uncertainties) added in quadrature. The disk parameters are then found via least squares minimisation, for which we use the modified blackbody,

$$F_\nu = nB_\nu(T_{\text{disk}})X_\lambda^{-1} \quad (1)$$

where  $n$  sets the overall level of dust with temperature  $T_{\text{disk}}$ , and

$$X_\lambda = \begin{cases} 1 & \lambda < \lambda_0 \\ (\lambda/\lambda_0)^\beta & \lambda > \lambda_0 \end{cases} \quad (2)$$

The blackbody function has units of  $\text{Jy sr}^{-1}$  so  $n$  is proportional to the surface area of dust in the disk. The fractional luminosity  $f_{\text{disk}} = L_{\text{disk}}/L_*$  of a given disk is therefore proportional to  $nT_{\text{disk}}^4$  (but also depends on  $X_\lambda$ ).

The physical origin of this formalism comes from the inability of grains to emit efficiently at wavelengths longer than their physical size. Therefore,  $\lambda_0$  is somehow related to grain sizes in the disk. It does not necessarily provide a direct measure of grain size however, because the observed emission comprises contributions from a size distribution of grains (which is related to  $\beta$ ).

After fitting a single blackbody, each disk spectrum is inspected for goodness of fit. In most cases where it is necessary, the need for a second temperature component is clear. However, we found that a formal criterion (such as  $\chi^2$ ) can be a poor indicator because there can be other reasons for a poor model fit that are unrelated to the number of temperature components.

For example,  $\zeta$  Lep shows evidence for extra emission above a blackbody around  $10\mu\text{m}$  (Fig. 2), which may be due to a silicate feature over the continuum, meaning that adding a second temperature component is not well justified based on the SED (mid-IR imaging suggests that the disk is somewhat

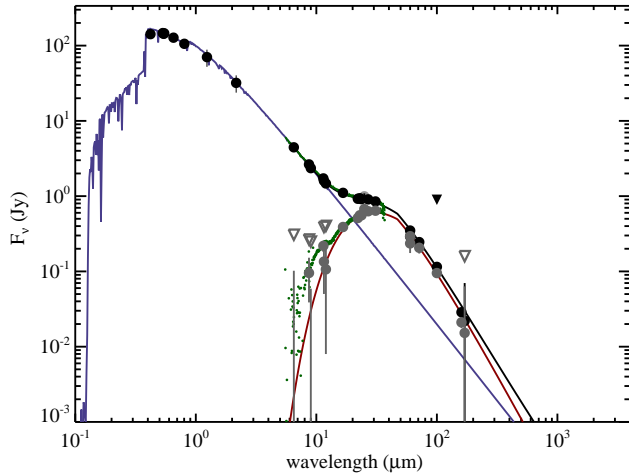


**Figure 2.** SED for  $\zeta$  Lep. Symbols are as described in Fig. 1. It is unclear whether the disk should be fitted as two temperature components, or whether the extra IRS emission near  $10 \mu\text{m}$  above the disk model (green dots above the red line) is due to non-continuum silicate emission.

extended, Moerchen et al. 2007). In some cases the issue may be a discontinuity in the IRS spectrum near  $15 \mu\text{m}$ , which is at the join between two different IRS modules and can cause a dip similar to that seen for  $\zeta$  Lep (Chen et al. 2009). In general, we err on the side of caution and include the two-temperature disks that appear to be the most robust. The only targets in our sample with strong silicate features are  $\beta$  Pictoris and  $\eta$  Corvi, for which the presence of two temperatures is clear and corroborated by other studies (see end of this section).

While we could allow a separate  $\lambda_0$  and  $\beta$  for the two components, these parameters are poorly constrained for the warmer component as the emission beyond the mid-IR is almost always dominated by the cooler component. We therefore fix  $\lambda_0$  and  $\beta$  to be the same for both components, and there are six model parameters to fit.

For objects that we do model with two temperatures, there remain degeneracies between the six parameters that are not necessarily well described by the covariance matrix that results from the least squares fitting. The most important is that disk temperature and normalisation are strongly correlated at constant total disk luminosity by the Stefan-Boltzmann law. To estimate the parameters and their uncertainties in a more robust way we use an ensemble Markov chain Monte-Carlo method (Goodman & Weare 2010)<sup>1</sup> using  $e^{-\chi^2/2}$  as our likelihood function. Chains with an ensemble of 200 “walkers” are initialised with parameters that vary randomly  $\pm 1\%$  from the  $\chi^2$  fitting results, and then run for 50 steps as a burn-in phase to eliminate any dependence on the initial state. This number of steps is sufficient to ensure the initial conditions do not influence the results, being at least ten times the autocorrelation length (Goodman & Weare 2010). The final distributions of parameters are created from a further 20 steps, resulting in 4000 samples from which we derive the probability distributions of each parameter.

<sup>1</sup> As implemented in the python emcee package (Foreman-Mackey et al. 2012).

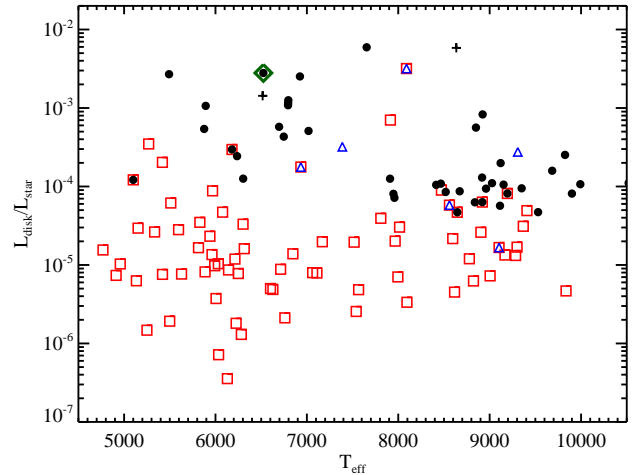


**Figure 3.** Sample of two-temperature disks (dots and triangles) and disks in the *Herschel* DEBRIS sample (squares). The nine dots and triangles enclosed by squares are DEBRIS stars with robust two-temperature disks. All disks are shown at their total fractional luminosity. The dot enclosed by a diamond is HD 181327, which Lebreton et al. (2012) show can be modelled with dust in a single narrow ring. Triangles note two-temperature systems found independently to have two disk components (see end of section 3). The two plus symbols show the single temperature disks, HD 191089 and HR 4796A, where two temperatures could easily have been detected but were not (see section 4.3).

Practically, rather than fit the component temperatures individually, we fit the temperature and normalisation of the cool component, and  $\lambda_0$  and  $\beta$  where sufficient photometry exists, and the ratio of warm to cool component temperatures

$$\mathcal{R}_T = T_{\text{warm}}/T_{\text{cool}} \quad (3)$$

and the ratio of warm to cool component normalisations  $\mathcal{R}_n$ . The ratio of fractional luminosities is

$$\mathcal{R}_f = f_{\text{warm}}/f_{\text{cool}}. \quad (4)$$

Here,  $\mathcal{R}_f$  is the preferable quantity to work with because  $\mathcal{R}_n$  and  $\mathcal{R}_T$  are strongly correlated by the Stefan-Boltzmann law, but any reasonable fit must produce a disk with roughly the same luminosity. We derive values and uncertainties by fitting a Gaussian to the marginalised distributions for each parameter.

We retain two-temperature disks as those where the temperatures of the warm and cool components are significantly different (i.e.  $\mathcal{R}_T > 3\sigma_{\mathcal{R}_T}$ ), and where the normalisation of the warm component is significantly different than zero (i.e.  $\mathcal{R}_n > 3\sigma_{\mathcal{R}_n}$ , all disks considered have significant cool components). The result of this process is a sample of 48 robust two-temperature debris disks. The targets are listed in Table A1 and the SEDs available in the online material. The overall fractional luminosities of these disks are shown in Fig. 3. Also shown are all disks for targets in the unbiased DEBRIS sample. The samples in this plot should not be used to conclude that two-temperature disks are typically brighter than other disks, or more common among bright disks, as significant biases exist among the two-temperature sample (see section 2 for a discussion of sample statistics).

Among our sample we also note systems where observations with sufficient spatial resolution have been able to show

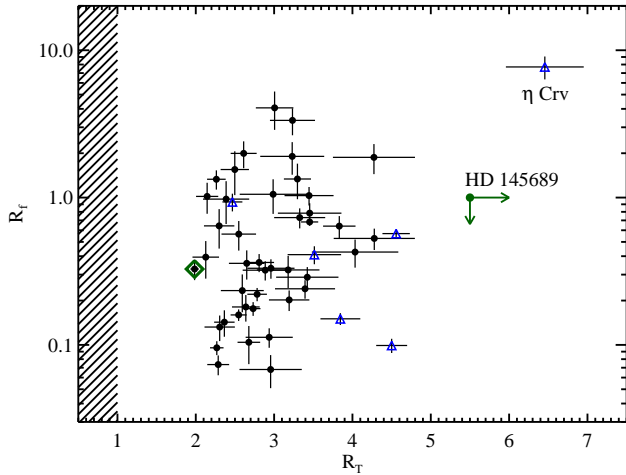


**Figure 4.** Two-temperature disks and uncertainties. Blue triangles note disks known to have multiple disk components from imaging and/or interferometry and the green diamond encloses HD 181327. The dot and arrow symbol marks HD 145689, host to an M9 companion, and for which  $\mathcal{R}_T$  is a lower limit (and  $\mathcal{R}_f$  an upper limit).

that two distinct disk components exist. These systems are Vega and Fomalhaut (Su et al. 2013),  $\eta$  Crv (Wyatt et al. 2005; Smith et al. 2009b; Duchêne et al. 2014), HR 8799 (Su et al. 2009; Matthews et al. 2014), and  $\eta$  Telescopii (Smith et al. 2009a). We also include  $\beta$  Pictoris in this list, where the disk is seen to extend over a wide range of stellocentric radii (e.g. Smith & Terrile 1984; Telesco et al. 2005).

## 4 RESULTS

A simple way to present two-temperature disks is the ratio of temperatures  $\mathcal{R}_T$  and fractional luminosities  $\mathcal{R}_f$ , as shown in Fig. 4. It is immediately clear that most two-temperature disks have fairly similar temperature ratios of 2-4, but with a range of fractional luminosity ratios. A clear outlier is  $\eta$  Crv, which has the largest temperature ratio, and is one of several systems known from detailed observations to have two physically distinct dust belts.

The source at intermediate  $\mathcal{R}_T$  is HD 145689, which has an unconstrained cool component temperature and is therefore plotted as a lower limit in  $\mathcal{R}_T$ . It is not formally part of our final two-temperature disk sample, but is mentioned here as a potentially interesting two temperature system found during our sample selection. As a probable outlier, we found it remarkable as the host of an M9 brown dwarf companion at  $6''.7$  (Huélamo et al. 2010). This source was proposed to be a  $\sim 40$  Myr old Argus star, and the disk model shown by Zuckerman et al. (2011) also has two temperature components. At 52 pc (van Leeuwen 2007) the minimum companion separation is about 350 AU. The disk radii implied by the two temperature fit of about 200 and  $< 35$  K are 7 and  $> 180$  AU respectively, though because these are estimates assuming blackbody grains, the distances are probably  $\sim 3$  times larger (Rodríguez & Zuckerman 2012; Booth et al. 2013). Therefore, if the  $70\mu\text{m}$  excess is associated with the star or companion, this system has three possible configurations (assuming that the larger than average temperature ratio is indeed indicative

of multiple belts). The primary may have two well-separated belts and the companion either orbits between or beyond the two belts. The third possibility is that the cool dust component actually orbits the companion, but is heated by the primary. HD 145689 is clearly an intriguing system, and proof of concept that Fig. 4 is a potentially powerful diagnostic for finding interesting planetary systems.

Aside from HD 145689, there is a simple demarcation between  $\eta$  Crv and the rest of our sample in Fig. 4. However, the sources at low  $\mathcal{R}_T$  are not all single-belt systems, as some that are otherwise known to have multiple dust populations are shown as blue triangles. These sit amongst the general population, perhaps adding strength to the standard assumption that multiple temperatures can always be interpreted as multiple dust belts.

Using the modelling results from Ballering et al. (2013) yields a very similar version of Fig. 4, with HD 145689 again a clear outlier (their sample did not include  $\eta$  Crv). A comparison using the modelling results of Chen et al. (2014) yields a very different plot, with  $\mathcal{R}_T$  covering a wide range and as high as 13 (the range of  $\mathcal{R}_f$  is similar). Their modelling finds two-temperature disks where we do not, and consistently hotter warm components. We suspect the origin of these differences lies with a difference between the 2MASS and *Spitzer* absolute calibrations, which we discuss further in section 4.3.

However, the young F6 star HD 181327 (the dot enclosed by a green diamond) is known to be concentrated in a relatively narrow single belt (Schneider et al. 2006). Lebreton et al. (2012) show that while the spectrum cannot be modelled with a single blackbody, allowing the composition of a narrow belt to vary can result in a good fit to the disk spectrum. Therefore, HD 181327 shows that not all two-temperature disks necessarily originate from two distinct components.

### 4.1 Sensitivity to two temperatures

We now consider the sensitivity to two-temperature disks in the parameter space shown in Fig. 4. Clearly, disks whose components have very different levels of emission will be hard to identify as having two components. Similarly, a warm component with a temperature approaching that of the star will be hard to detect photometrically (i.e. these are usually detected with interferometry), so stars with very large temperature ratios will also be hard to detect. Of course, sufficiently small temperature ratios will also be impossible to discern as comprising multiple temperatures. Combined, these criteria mean that there should be bounds on all sides of Fig. 4 that limit the range of two-temperature disks that can be discovered. The fainter the disk overall, the lower the S/N of all measurements will be in general, and therefore the less parameter space these bounds will cover.

To quantify this picture in a little more detail, Fig. 5 shows a simple approximation of the regions in which a “typical” set of observations could detect two-temperature emission. At each point in the parameter space covered, we generated two pure blackbodies, with a fixed 70 K cool component, varying  $\mathcal{R}_T$  to set the warm component temperature, and then “observed” them with synthetic photometry at seven IRS (4-35  $\mu\text{m}$ ), three MIPS (24-160  $\mu\text{m}$ ), and two SCUBA (450-850  $\mu\text{m}$ ) bands. We peak-normalised each total spectrum to unity, and estimated the uncertainties as  $0.01 F_\nu^{1/4}$ , which corresponds to 1% uncertainty

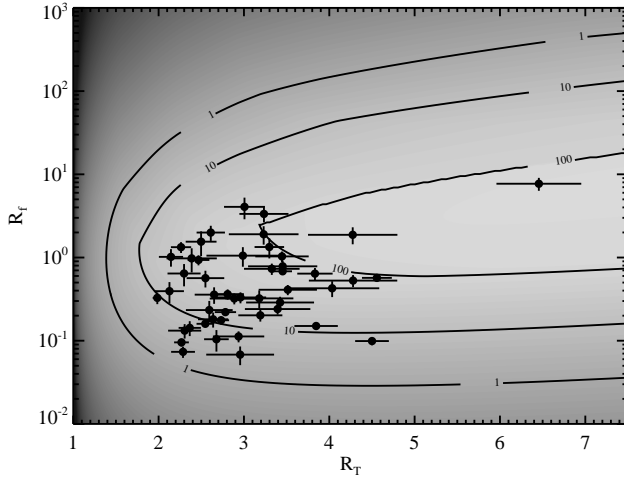


**Figure 5.** Simple model of sensitivity to two temperature excesses, where lighter grey corresponds to greater sensitivity. Contours show  $\chi^2_{\text{red}}$  from fitting a single temperature blackbody to two-temperature disks with the parameters at each point in the parameter space. Disks near the  $\chi^2_{\text{red}} = 1$  contour are well described by a single blackbody, and therefore two temperature disks with these properties cannot be discovered given observations with typical S/N. The lowest  $\mathcal{R}_f$  and  $\mathcal{R}_T$  two-temperature disks lie near the edge of detectability, suggesting that disks with  $\mathcal{R}_T \lesssim 2$  and  $\mathcal{R}_f \lesssim 0.1$  do exist but were not detected here. Similarly, two temperature disks near  $\mathcal{R}_T \sim 5 - 6$  and  $\mathcal{R}_f \sim 1 - 10$  are easily detected, so the gap between most disks and  $\eta$  Crv is real. Disks with  $10 \lesssim \mathcal{R}_f \lesssim 100$  and  $\mathcal{R}_T \gtrsim 2$  are detectable but were not seen, so must be rare.

at the peak, and 32% (i.e. a  $3\sigma$  upper limit) for measurements two orders of magnitude fainter. We additionally set the minimum uncertainty to be 5%. While this prescription simplifies the realities of photometry collected from different instruments with many different observing strategies, it represents the limits reasonably well (e.g. see Figs. 1 and 2). To each spectrum we fit a single blackbody and computed the sum of squared deviations per degree of freedom ( $\chi^2_{\text{red}}$ ), which are the contours shown in Fig. 5.

In darker regions where  $\chi^2_{\text{red}}$  is low (i.e.  $< 1$ ) a single blackbody is a good model of the emission, and a two-temperature disk cannot be confidently detected. In lighter regions where  $\chi^2_{\text{red}}$  is higher, two-temperature disks are easier to detect. We have also shown the two-temperature disks from Fig. 4 (except HD 145689), which shows that the simple detection simulation is reasonable in the sense that no two-temperature disks lie where they should not be detectable. Fig. 5 shows that the most simple criterion for detecting two temperature disks is that one component does not dominate over the other, and that their temperatures are not too similar.

Two-temperature disks are harder to detect in overall fainter disks, simply because their measurements are typically less precise. For the same photometric precision, lowering the overall disk brightness by a factor of three results in uncertainties that are three times larger. In Fig. 5, the  $\chi^2_{\text{red}}$  contours would therefore be divided by a factor of nine and disks with  $\mathcal{R}_f$  lower than about 0.2 become harder to detect. We return to the effect of this disk luminosity bias when looking at spectral type trends below.

Our simulation does not include a limit at large temperature ratios because these are limited not by the disk properties,

but by difficulties in distinguishing the warm component from the star. Because disks are rarely cooler than  $\sim 30\text{K}$ , and disks hotter than  $\sim 500\text{K}$  become increasingly difficult to detect with photometry, the practical upper limit on detectable temperature ratios is in the 15-20 range (depending on the temperature of the cool component).

The conclusions from this analysis are i) that the lowest  $\mathcal{R}_f$  and  $\mathcal{R}_T$  disks lie near the sensitivity limits, meaning that disks with lower  $\mathcal{R}_f$  and  $\mathcal{R}_T$  probably exist, but were not detectable here, ii) that two-temperature disks are harder to detect when the overall disk luminosity is lower, iii) that disks with  $10 \lesssim \mathcal{R}_f \lesssim 100$  and  $\mathcal{R}_T \gtrsim 2$  are detectable but were not seen, so must be rare, and iv) the gap between most disks and  $\eta$  Crv is in a region where two-temperature disks are most easily detected, so the gap is real and the  $\eta$  Crv disk is a rare outlier among two-temperature disks.

## 4.2 Trends with spectral type

Fig. 6 shows how some of the derived disk parameters vary with stellar effective temperature, as well as approximate biases due to the sensitivity to two temperatures described above. Chen et al. (2014) analysed a much larger sample of stars observed with IRS, and found similar trends, though they did not present the results in terms of the ratios we use here.

The temperature of the cool component increases with  $T_{\text{eff}}$ , as might be expected due to increasing stellar luminosity if all disks have similar characteristic sizes (see Ballering et al. 2013, for further discussion of this trend). Because  $\mathcal{R}_T$  is generally similar for all stars, the warm component temperatures show the same trend. This conclusion is in contrast to Morales et al. (2011), who found that the warm component temperature was generally constant, regardless of spectral type (also see Chen et al. 2014). However, plotting their temperatures shows a probable correlation, with all Sun-like stars having warm components  $< 220\text{K}$ , but 15 out of 24 A-type stars having warm components  $> 220\text{K}$ . Indeed, their A-type sample contains stars that range from B8 to A7 and there is also a trend among these for the hotter stars to have warmer warm excesses. A possible bias exists here however, because for fixed sensitivity to  $\mathcal{R}_T$ , increasing cool belt temperatures mean that only warm belts with increased temperatures can be detected. A predicted detection line of  $\mathcal{R}_T \gtrsim 2$  is shown in the lower left panel of Fig. 6, based on the lower envelope of temperatures in the lower right panel. The lowest warm temperatures around the hottest stars lie farther above the detection line than would be expected, so it seems likely that the trend towards warmer warm belts around hotter stars is real. There is no such bias for the top envelope of points in any of the panels, so the observed increase in the warmest warm component temperatures with stellar temperature also argues that the trend is real. Our interpretation of both sets of two-temperature fitting results is therefore different to the Morales et al. (2011) conclusion of common warm dust temperatures, instead finding a probable trend for warmer dust around hotter stars.

While the maximum  $\mathcal{R}_f$  appears to be constant, the minimum  $\mathcal{R}_f$  appears to increase with  $T_{\text{eff}}$ , and the hottest stars tend to have similarly luminous warm and cool components. This trend may be a bias however, as the hotter stars in our sample tend to have lower overall fractional luminosities (Fig. 3),

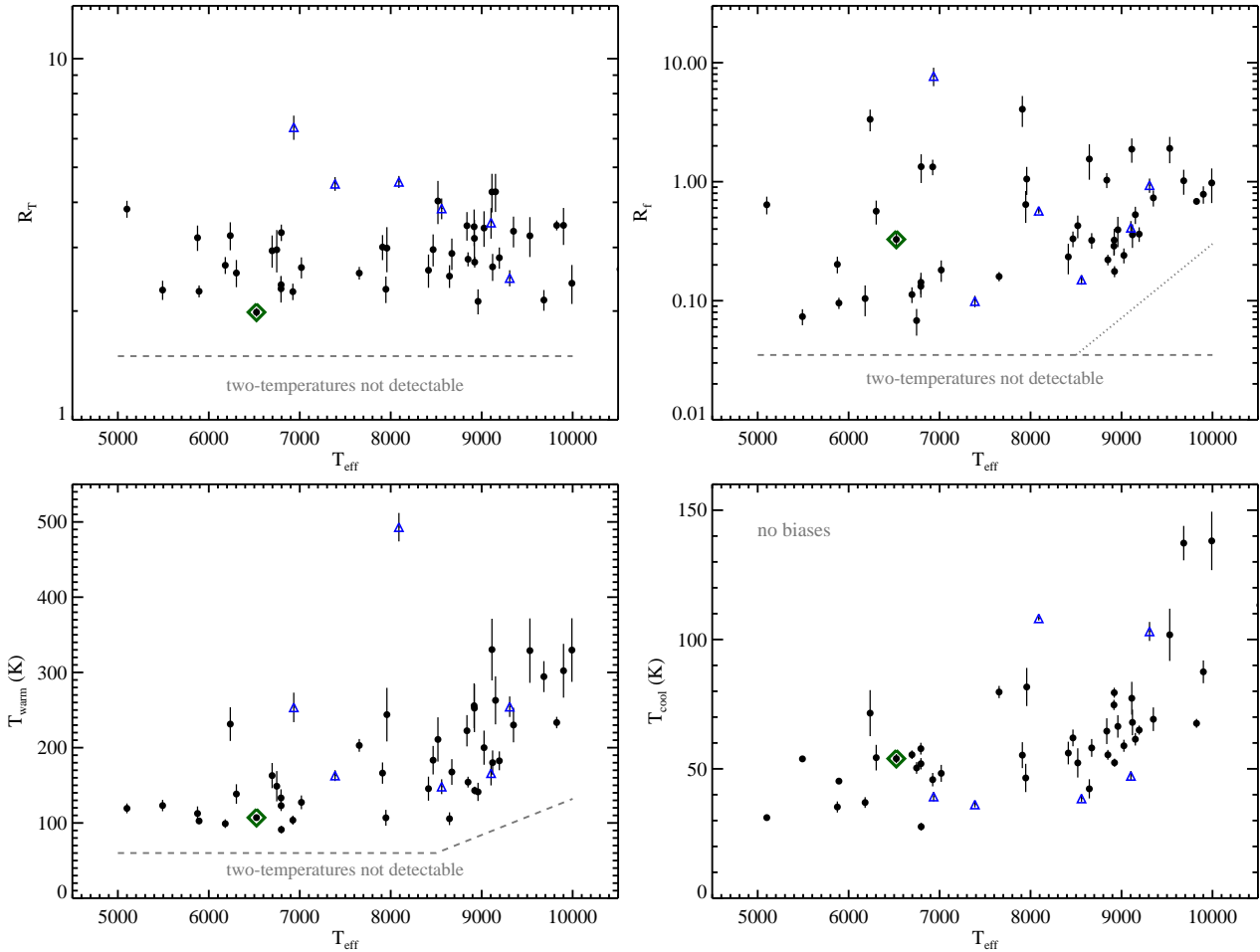


**Figure 6.** Relations between  $\mathcal{R}_T$ ,  $\mathcal{R}_f$ ,  $T_{\text{warm}}$ ,  $T_{\text{cool}}$  and stellar effective temperature. Blue triangles note disks known to have multiple disk components from imaging and/or interferometry and the green diamond encloses HD 181327. Biases derived in Fig. 5 (see section 4.1) are shown by dashed lines, with an additional possible bias arising from disks being fainter overall around hotter stars shown by the dotted line. There are no biases that affect the upper envelope of points in these plots.

for which detecting low  $\mathcal{R}_f$  disks is more difficult (as indicated by the dotted line in the upper right panel).

### 4.3 Disks with single temperature spectra

As we have emphasised, to be sure that a debris disk comprises multiple components requires at least one of those components to be resolved. For example, disks with well-resolved outer belts such as Fomalhaut and Vega show unresolved emission closer to the star at  $\sim 10$  au, strong evidence for multiple belts that in these cases is consistent with their two-temperature SEDs (Su et al. 2013).

There are however, also disks that show both warm and cool emission from imaging but appear to have single temperature disk spectra. For example,  $\alpha$  CrB is resolved in both mid-IR and far-IR imaging, suggesting that the disk has either two belts, or a disk that extends over a wide range of radii, yet the SED is well fit by a single modified blackbody (Moerchen et al. 2010; Kennedy et al. 2012). An intermediate class also exists, where the disk spectra are sufficiently complicated by spectral features that a poor single temperature fit does not immediately suggest that a two-temperature model would be better (e.g. Fig.

2). As another example, the HD 113766A disk spectrum can be modelled moderately well as a single component, but when considered in light of mid-IR interferometry, the combined photometry shows that a two-belt model is a better interpretation (Olofsson et al. 2013).

An additional question is whether there are disks where two-temperature behaviour was not detected where it could have been, or stated another way; do all disks have two temperatures? While it does not have two temperatures, a disk such as that around HD 113766A is not particularly well suited for this test because it has strong spectral features. Two that are well suited are HD 191089 and HR 4796A, as shown in Fig. 7. Both disks are extremely bright ( $f = 0.001 - 0.006$ ) and given the high S/N are very well modelled by modified blackbodies at about 100K. From the range of  $\mathcal{R}_T$  and  $\mathcal{R}_f$  at the effective temperatures of 6500 and 8630K, Fig. 6 shows that a typical warm component would have  $T_{\text{warm}} = 200 - 400\text{K}$  and  $f = 10^{-4}$  to  $10^{-2}$ , which would have been easily detected. Fig. 5 suggests that warm disks in this temperature range would still be detectable if they were up to an order of magnitude fainter.

For HD 191089, Churcher et al. (2011) concluded from mid-IR imaging that the inner regions were truly depleted, sug-

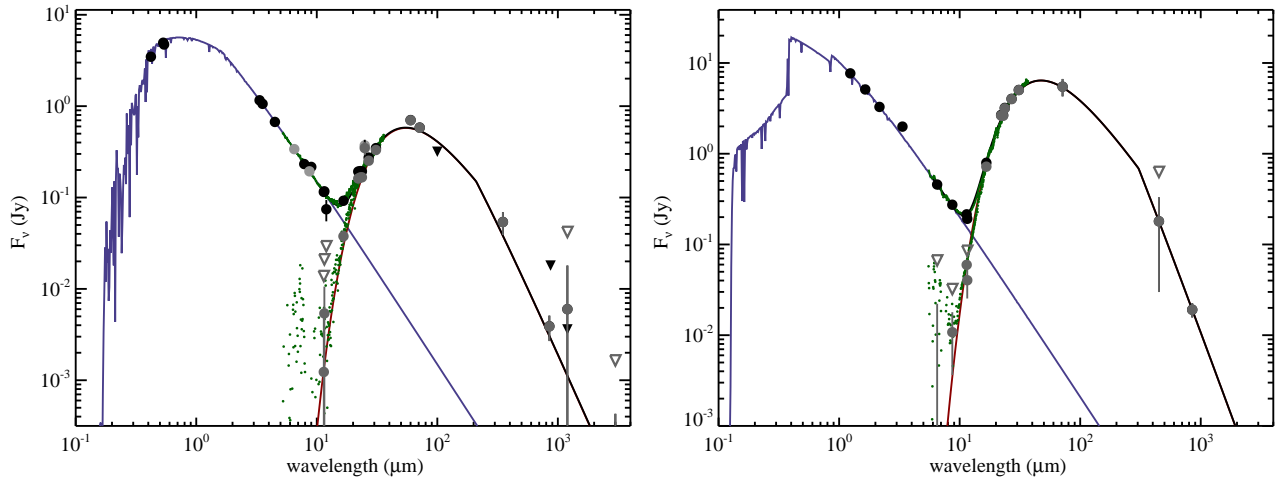


**Figure 7.** SEDs for the single-temperature systems HD 191089 (left) and HR 4796A (right). Black dots and triangles show photometry and upper limits, and grey dots and triangles show star-subtracted photometry and upper limits. The green line and dots show the observed and star-subtracted IRS spectra. The blue line shows the stellar photosphere model, the red lines the individual and total disk emission, and the black line the star+disk emission.

gesting that in addition to appearing as a single temperature disk, that the emission does actually come from a single belt. Our result of a single temperature is in contrast to the two temperature model of Chen et al. (2014), which they strongly prefer. However, this appears to be an artefact of their analysis, which decreases the MIPS  $70\mu\text{m}$  uncertainties by a factor of 70. Our inclusion of longer wavelength photometry shows that the second temperature component is not justified.

Detailed modelling of HR 4796A requires two spatially distinct dust belts (Augereau et al. 1999; Wahhaj et al. 2005). Again our model is in disagreement with Chen et al. (2014), who find a warm temperature component at 231K. The main difference between our methods is that we tie our IRS spectra to the photosphere, whereas Chen et al. (2014) tie it to MIPS  $24\mu\text{m}$  photometry, which requires an accurate relative calibration between the photosphere models and MIPS data. Inspection of the distribution of 13 and  $24\mu\text{m}$  observed/star flux ratios from their Table 2 provides a possible resolution; near unity their distributions have means of 1.02 and 1.03 respectively, suggesting that the photospheres are on average underestimated relative to IRS. A possible origin of this discrepancy is that the 2MASS photometric system is about 2% fainter than that used by MIPS (Rieke et al. 2008), which if not corrected for will lead to slightly fainter photospheres and the inference of warm disk components where the evidence is marginal.

Chen et al. (2014) find that there are many other examples of single temperature disks. Therefore, not all stars have strong evidence for two-temperature disks even when they could have been detected, and single temperature disks may or may not actually have multiple belts.

#### 4.4 Statistics

Given that many two-temperature disks are known to exist, it is desirable to make an estimate of how common the phenomenon is. Ultimately we are biased by the overall set of stars that were observed with IRS, since among nearby stars these were typically those already known to host bright disks, and we are there-

fore biased towards detecting two-temperatures in general. This bias means that any simple estimate of the two-temperature occurrence rate will very likely be an overestimate.

We first consider stars in the unbiased DEBRIS sample (i.e. including stars observed by DUNES and with guaranteed time). Only one of these was observed by the Morales et al. (2009) programme (HD 110411), meaning that objects in this sample observed with IRS are unlikely to be strongly biased towards having two temperatures (see section 2). Our sample of two-temperature disks has 9 DEBRIS stars (6 A-type, 2 F-type, 1 K-type), while the DEBRIS sample itself has 83 A-type, 94 F-type, 89 G-type, 91 K-type, and 89 M-type primary stars. Of these, 21, 17, 9, 6, and 1 were observed with IRS and have detected disks respectively, meaning that the raw fractions of disks that have two-temperatures are 6/21, 2/17, 0/9, 1/6, and 0/1.

Fig. 3 shows how our overall sample of two-temperature disks compares to the DEBRIS sample. The volume-limited DEBRIS sample includes relatively few bright disks (as these are rare), and only the brightest DEBRIS disks are seen to have two temperatures. However, the fainter disks may have two-temperature components that could not be detected. A lack of sensitivity may therefore account for only a few (3/32) two-temperature disks among FGK stars in DEBRIS. With the above caveat about a bias towards two temperatures among IRS-observed disks, this fraction suggests that two-temperature disks are fairly common around FGK stars. For A-types, there is still little overlap in the two-temperature and DEBRIS stars in Fig. 3, but nearly 30% of A-star disks are seen to have two temperatures. Further, Fig. 6 shows that these disks tend to have higher  $\mathcal{R}_f$ , meaning that it is likely that some of the remaining 70% of DEBRIS A-type disks should have detectable two-temperature behaviour that was not seen. Therefore, this largely qualitative look at two-temperature disks among DEBRIS stars suggests that the phenomenon could be relatively common, at a level of a few tens of percent.

To approach this issue from another angle, we consider the brightest disks observed with IRS by Chen et al. (2006), those with overall fractional luminosities above  $10^{-3}$ . These



six disks are all around stars younger than  $\sim 20$  Myr old, and are sufficiently bright that two-temperature disks similar to others in our sample should have been easily detectable. These are HD 95086, HD 110058, HD 113766, HD 146897, HD 181327, and HD 191089. Of these, HD 95086 and HD 181327 show two temperatures (Lebreton et al. 2012; Moór et al. 2013), while the other four do not. HD 113766 has a silicate feature that makes SED fitting complex, but is inferred to have two spatially distinct components (Olofsson et al. 2013). Therefore, one third of this small number of stars with disks show two temperatures.

This rough estimate is lower than the 66% found by Chen et al. (2014), and in closer agreement with 46 and 33% found by Morales et al. (2011) and Ballering et al. (2013). There seem to be three possible reasons for this difference. The first two are related to the way Chen et al. (2014) model their disk spectra, which may result in detection of more two-temperature disks as described above in relation to HD 191089 and HR 4796A. A third possible reason is the difference in samples, because Chen et al. (2014) include many young stars. They found that younger systems are more likely to have two-temperature disks, which may increase their detection rate of two-temperature disks, particularly if many of these young stars were observed based on previous disk detections.

Another question is therefore whether the frequency of two-temperature disks changes with age, or whether they are just easier to detect due to brighter disks at younger ages. For example, if the warm components are related to ongoing terrestrial planet formation and are independent of the outer cool components, then two-temperature disks would only be expected to appear around stars younger than  $\sim 100$  Myr. We can therefore compare our rough two-temperature occurrence rates from DEBRIS and the younger Chen et al. (2006) sample. Though our power to distinguish them is limited, there is no evidence among these samples that the fraction of two-temperature disks changes with age. Though they did not consider this possibility, Fig. 9 from Chen et al. (2014) suggests that the frequency of two-temperature disks is generally fairly constant, but could be higher for systems younger than  $\sim 10$  Myr. We consider this issue in more detail in section 6.2.

To summarise, the results do not rule out two-temperature behaviour for most disks, because most are too faint for it to be detected reliably. We have also shown that there are examples of single temperature disks where two temperatures could have been detected. Based on this discussion it seems that two-temperature disks are certainly not rare, but neither are they ubiquitous.

## 5 THEORETICAL GRAIN MODELS

Having studied the observational properties of two-temperature disks, we now explore how two-temperature emission might appear from a dust belt at a single radial distance  $r$  from the central star. These ideas largely rely on the differences in temperature that grains of different sizes can have at a single stellocentric radius, which we consider first. We then move on to numerical models, whose spectra in general depend on the host star, the grain size distribution, and the optical properties of the grains.

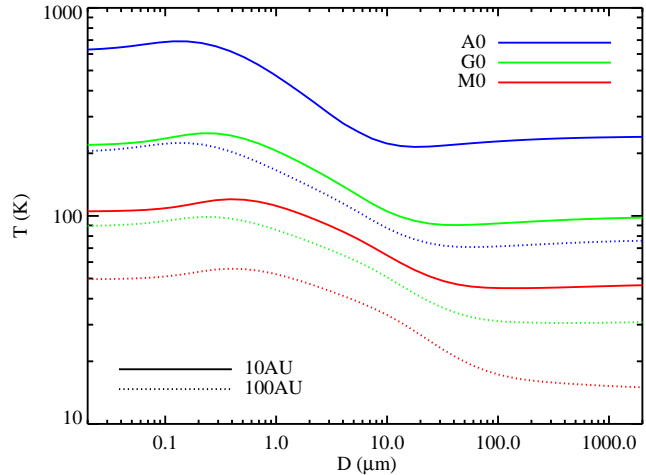


**Figure 8.** Grain temperatures as a function of diameter for dust around A, G, and M-type stars at 10 and 100AU. The temperature ratios for small and large grains in this figure vary from 2.2 to 3.3. The grain model is described in section 5.2.1.

### 5.1 Grain temperatures

Fundamentally, two-temperature emission could arise from single dust belts because the temperature of dust grains depends on their size, as shown in Fig. 8. There are two temperature regimes separated by a transition region; the cooler blackbody regime is where grains are large and absorb and emit efficiently at all wavelengths, and the “small” regime is where grains absorb and emit inefficiently at all wavelengths. The exact location of these regimes depends on the spectral type of the star and the radial location of the dust, but is a fairly weak function of these parameters. Fig. 8 shows that while the temperatures vary considerably with spectral type and radial distance, the ratio of temperatures in the small ( $T_{\text{sm}}$ ) and blackbody ( $T_{\text{BB}}$ ) grain regimes is fairly constant at around 2-3.

To understand this ratio theoretically we balance the energy absorbed by a dust particle of diameter  $D$  over area  $\pi D^2/4$  and emitted from an area  $\pi D^2$  at stellocentric distance  $r$

$$\frac{R_*^2}{4r^2} \int_0^\infty Q_{\text{abs}} B_\nu(T_*) d\lambda = \int_0^\infty Q_{\text{abs}} B_\nu(T_{\text{dust}}) d\lambda. \quad (5)$$

For a blackbody particle that is perfectly absorbing and emitting  $Q_{\text{abs}} = 1$  and the blackbody dust temperature is

$$T_{\text{BB}}^4 = \frac{T_*^4 R_*^2}{4r^2} = \frac{L_*}{16\sigma_K \pi r^2} \quad (6)$$

where  $\sigma_K$  is the Stefan-Boltzmann constant.

If we now consider a grain that is small relative to the peak wavelengths of star and disk emission, the absorption and emission efficiency is  $Q_{\text{abs}} \propto \lambda^{-n}$  at wavelengths that contribute significantly to the integrals in Eq. (5). For fixed  $n$  these integrals are  $\propto T^{4+n}$ , so Eq. (5) can be rewritten as

$$\frac{T_{\text{sm}}}{T_{\text{BB}}} = \left( \frac{T_*}{T_{\text{BB}}} \right)^{n/(4+n)}. \quad (7)$$

For typical values of  $n = 1-2$  (e.g. Helou 1989),  $T_* = 6000\text{K}$ , and  $T_{\text{BB}} = 70\text{K}$ , equation (7) yields  $T_{\text{sm}}/T_{\text{BB}} = 2.4 - 4.4$ , which is in good agreement with the ratios found in Fig. 8.

These values are therefore representative of the temperature ratios  $\mathcal{R}_T$  that are achievable in a two-temperature debris

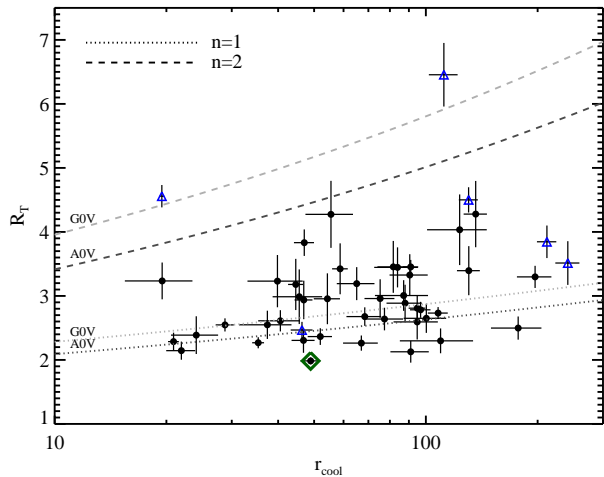


**Figure 9.**  $\mathcal{R}_T$  as a function of  $r_{\text{cool}}$ . A weak positive correlation is predicted by Eq. (7), shown for A0V and G0V stars for  $n = 1$  and 2.

disk with dust in a single belt. While the observed ratios could be smaller, if for example the smallest grains present in the disk were  $\sim 10\mu\text{m}$  in size and therefore grains of  $T_{\text{sm}}$  nonexistent, they cannot be larger than allowed by the grain properties. If we take  $T_{\text{sm}}/T_{\text{BB}} = 5$  as an approximate maximum allowed value, then  $\eta$  Crv with  $\mathcal{R}_T = 6.4$  is the only source for which the conclusion of two spatially distinct belts would be well founded based purely on these simple temperature considerations.

Eq. (7) also predicts a weakly increasing temperature ratio with disk radius (via  $T_{\text{BB}} \propto \sqrt{r}$ ). Fig. 9 shows  $\mathcal{R}_T$  against disk radius in search of this trend, with lines showing the predicted correlation. No clear trend is visible, and the scatter in the points is larger than the variation expected for  $n = 1$ . The expected trend for  $n = 2$  is larger, but as comparison with Fig. 8 shows,  $n = 2$  tends to overestimate values for  $\mathcal{R}_T$  so is probably too extreme to be representative. Inspection of this plot as a function of spectral type shows no trends, though the relatively small difference between lines of different spectral types shows that the expected differences are small. Therefore, this comparison shows that a possible  $\mathcal{R}_T$  dependence on  $r_{\text{cool}}$  is not a good diagnostic of two-temperature disks that may arise from the range of grain temperatures in a single belt.

There is one more important aspect to be explored before turning to a more complex model, which is the minimum grain size. The conclusion that any disk with  $\mathcal{R}_T \lesssim 5$  can be produced by a single dust belt relies on grains smaller than  $\sim 1\mu\text{m}$  being able to survive in the disk. However, it is thought that such small grains are blown out by radiation pressure on dynamical timescales for Sun-like and earlier-type stars. Adopting the relation for the blowout size in microns

$$D_{\text{bl}} = 0.8(L_*/M_*)(2700/\rho), \quad (8)$$

where  $\rho$  is density in  $\text{kg m}^{-3}$  and the luminosity and mass are in Solar units, implies that while Sun-like stars can retain grains that are small enough to achieve  $T_{\text{sm}}$ , A0-type stars with typical blowout sizes of  $10\mu\text{m}$  do not. Therefore, a conclusion from Fig. 8 is that early A-type stars only retain grains that are all roughly the temperature of a blackbody. Therefore, if the calculated blowout size is representative of the minimum grain size, early A-stars should not show two-temperature spectra from a single dust belt. Another conclusion is that the minimum grain

size for Sun-like stars is sufficiently small that two-temperature spectra from a single belt are possible.

## 5.2 Numerical models

Having considered the possible range of grain temperatures, we now consider what is probable given realistic size distributions and compositions. The size distribution can be reasonably approximated by a power-law with a single slope parameter, while the optical properties require a handful of parameters that describe the material composition.

### 5.2.1 Model description

In what follows we use a fairly standard grain composition model (Augereau et al. 1999). In this model all grains have the same basic properties, and are some mix of crystalline/amorphous silicates and organics with some porosity, where the vacuum arising due to the porosity can be filled to some degree with crystalline or amorphous water ice. Grain properties are calculated using Mie or Rayleigh-Gans theory or geometric optics in the appropriate regimes (Laor & Draine 1993), using optical properties derived by Li & Greenberg (1997, 1998). The refractive indices of each material are mixed according to Maxwell-Garnett effective-medium theory, which is not the only choice, but was preferred because it allows the grains to be treated as a silicate core with a mantle of organics (i.e. the components are not treated equally when mixed). This grain model is not the only possible approach, and for example has problems reproducing observations when confronted with debris disks observed both in thermal and scattered light (e.g. Krist et al. 2010; Acke et al. 2012). However, it has succeeded in many instances when modelling of mid to far-IR disk spectra was required (e.g. Augereau et al. 1999; Wyatt & Dent 2002; Lebreton et al. 2012), and provides a unified approach that has proven a useful tool for creating models more realistic and complex than simple blackbodies.

Even with the various assumptions that were made in creating this grain model, there are several more to be made. As outlined above, the minimum grain size and the size distribution are important in setting the disk spectrum. We must also specify the mixture of silicates, organics, vacuum (via porosity), and water ice (if the porosity is non-zero), and whether these are crystalline or not. Formally,  $q_{\text{si}}$  sets the fraction of total silicate+organic volume occupied by silicates,  $p$  the porosity fraction, and  $q_{\text{H}_2\text{O}}$  the fraction of vacuum filled with ice. We set the blowout size as the size at which the radiation to gravitational force ratio parameter  $\beta$  is 0.5.

For the composition, we use two different models that illustrate how the disk spectra can vary. While previous authors (e.g. Augereau et al. 1999) have used compositions at different extremes of what is possible, for example interstellar medium-like and comet-like to explore how disk spectra can vary, we found that crystalline comet-like compositions produced disks with strong spectral features that are not seen among our sample. Our two compositions are therefore not so extreme. We default to moderately porous grains with 1/3 amorphous silicates and 2/3 organics, and a small amount of water ice (i.e.  $p = 0.5$ ,  $q_{\text{si}} = 1/3$ ,  $q_{\text{H}_2\text{O}} = 0.05$ ), which we call our “rocky” composition. For a second model, we increase  $q_{\text{H}_2\text{O}}$  to 0.85, which we call the “icy” composition.

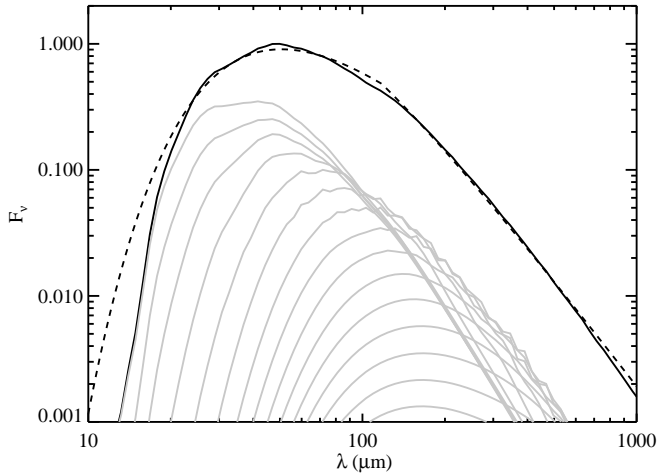


**Figure 10.** Disk spectrum for  $r = 100$  AU around a Sun-like star with our “rocky” composition and  $q = 1.9$ ,  $D_{\text{bl}} = 3\mu\text{m}$ . The maximum object size is 1km. The solid black line shows the total spectrum, solid grey lines show the contribution from 15 logarithmically-spaced size bins (from  $3\mu\text{m}$  to 40mm with a factor of 1.96 spacing). Pebbles larger than 40mm lie off the bottom of the plot. The dashed line shows a 106K blackbody with  $\lambda_0 = 123\mu\text{m}$  and  $\beta = 0.88$ .

Above, we considered the possible range of temperatures that could be present in a dust belt. However, how different sizes contribute to the overall emission is set by the size distribution, so unless it allows both the coolest and warmest grains to contribute roughly equally to the emission, the presence of multiple dust temperatures will not result in a two-temperature disk spectrum. One common way of describing the number of objects between diameters  $D$  and  $D + dD$  in the size distribution is

$$n(D)dD = KD^{2-3q}dD, \quad (9)$$

where  $K$  sets the normalisation and  $q$  the steepness of the distribution (the origin of  $q$  being in the mass distribution  $n(M)dM \propto M^{-q}dM$ ). When  $q > 1.67$  the surface area is dominated by the smallest particles. A standard value for  $q$  under the assumption of an infinite size distribution with strength-independent size is 1.83 (Dohnanyi 1969). However, the slope  $q$  varies depending on the size-dependent strength of objects (O’Brien & Greenberg 2003), with typical values expected to be around 1.8-1.9 for objects that dominate the observable emission (e.g. Gáspár et al. 2012).

### 5.2.2 Model results

We now show disk spectra for single-belt models with a range of size distributions and our two compositions. We first show why changing the size distribution has important consequences for the disk spectrum, and then how these models compare to the observed sample of two-temperature disks for a range of size distributions and our two compositions.

We begin this part of the analysis with Fig. 10, which shows a typical disk spectrum using the “rocky” composition with  $q = 1.9$  at 100AU from a Sun-like star with the solid black line. The resulting spectrum is well matched by a modified blackbody beyond  $20\mu\text{m}$  (dashed line). No two-temperature behaviour is present and if anything, the blackbody model has too

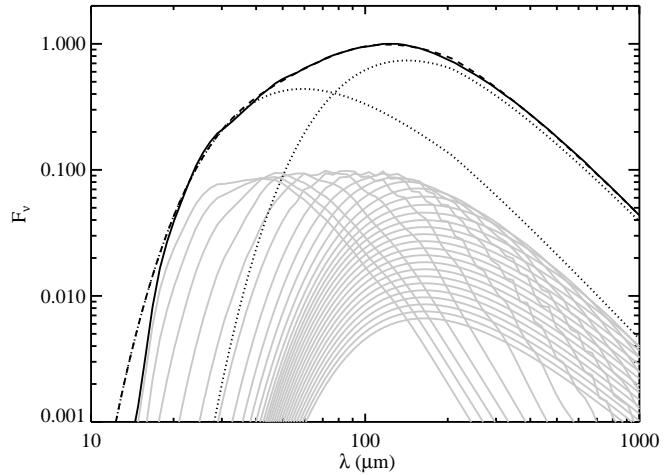


**Figure 11.** Same as Fig. 10, but with  $q = 1.73$ . The model has temperatures of 36 and 86 (dotted lines, with  $\mathcal{R}_T = 2.6$ ) and  $\mathcal{R}_f = 1.8$ , with  $\lambda_0 = 206\mu\text{m}$  and  $\beta = 0.35$ . The flatter size distribution means that large objects, even those with 1 km diameters, contribute significantly to the overall spectrum.

much warm emission rather than too little. What is also clearly visible is that the emission is made up of a range of temperature components (grey lines), to the extent that it is perhaps remarkable that the overall spectrum is well described by a modified blackbody. The size distribution of  $q = 1.9$  means that the spectrum contains a reasonable balance of these temperature components and the overall spectrum has a temperature that is somewhere between  $T_{\text{sm}}$  and  $T_{\text{BB}}$ .

To create a disk spectrum that looks more like it has two temperatures will require different relative numbers of small and large grains. Decreasing the contribution from large grains will only push the spectrum further towards something that looks like a modified blackbody at  $T_{\text{sm}}$ . However, increasing the number of large grains can result in a more even contribution and a broader spectrum, as shown in Fig. 11. This figure shows the result if  $q = 1.73$ , which clearly shows a two-temperature spectrum. The two-blackbody fit has  $\mathcal{R}_T = 2.6$  and  $\mathcal{R}_f = 1.8$ , which lies amongst the disks shown in Fig. 4, though with a relatively high  $\mathcal{R}_f$ . Some experimentation shows that two-temperatures are required to fit our grain model SEDs for Sun-like stars when  $q \lesssim 1.8$ , and that similar results can be obtained using either our rocky or icy compositions. As noted above, this scenario does not work for early A-type stars, as long as we retain the assumption that sub-blowout size grains do not make a significant contribution to the disk spectrum.

To illustrate the range of behaviour and the trends that arise from these relatively steep size distributions, Fig. 12 shows models with our rocky composition ( $q_{\text{H}_2\text{O}} = 0.05$ ) for a range of size distributions ( $q = 1.68, 1.72, 1.77, \text{ and } 1.82$ ) and spectral types (A5, F0, G0, and K0) with fitted blackbody models. We use the same assumptions for fitting blackbody models as in Fig. 5, but now fit two temperature components. The second fitted component is not shown if it has the same parameters as the first. Some trends are clear;  $\mathcal{R}_f$  tends to increase with the steepness of the size distribution, which can be understood simply as a result of the decreasing contribution of the large grains. The typical  $\mathcal{R}_T$  increases to later spectral types, which is the

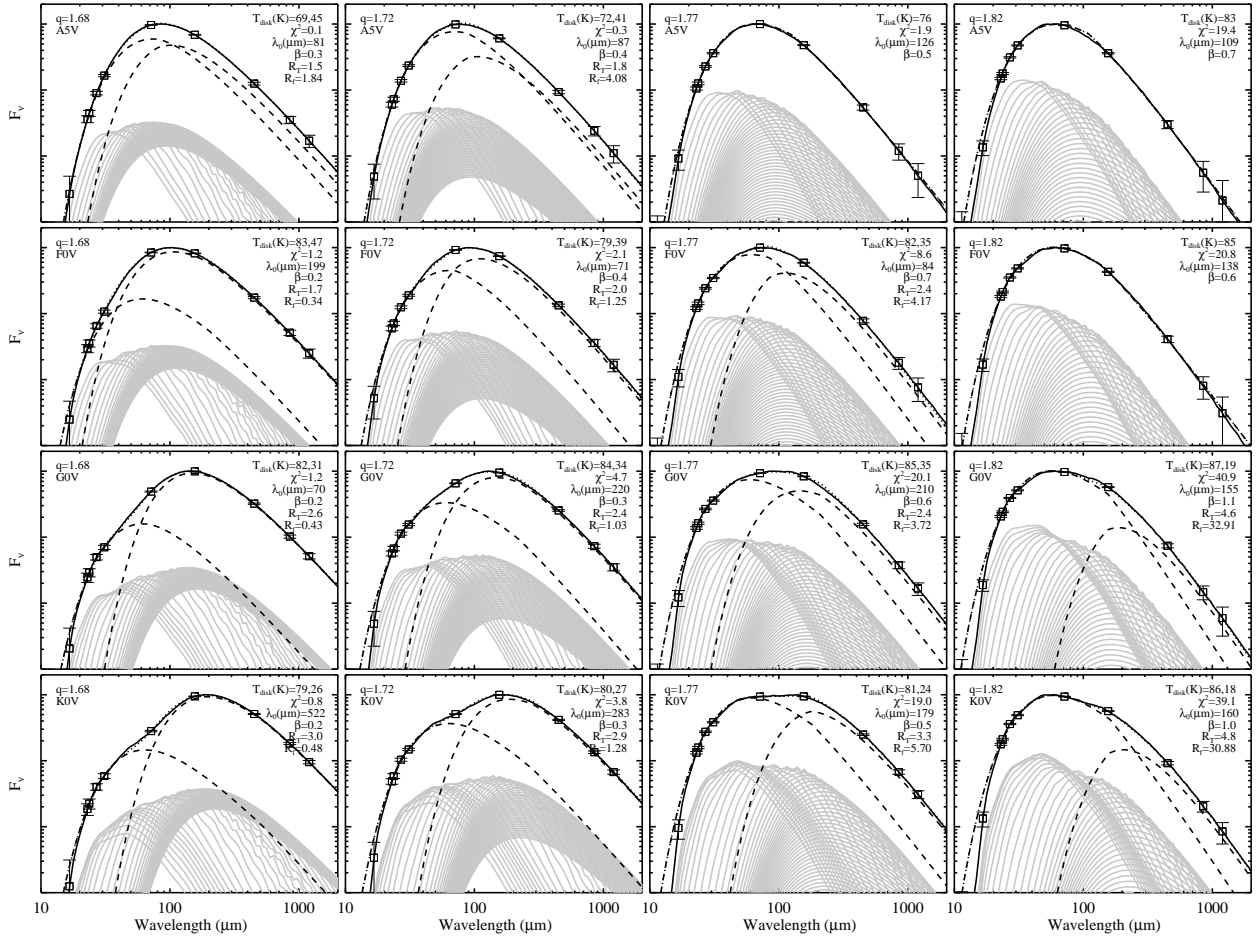


**Figure 12.** Example two-temperature disk spectra for a range of spectral types and size distribution slopes (noted in the top left of each panel), assuming that the minimum grain size is the blowout size and with our “rocky” composition ( $q_{\text{H}_2\text{O}} = 0.05$ ). All disks are at 100 au. Each panel shows the contribution of grains of different sizes (grey lines) and the total spectrum (solid line). The best-fit two-temperature blackbody model is shown (dotted line), as is each component (dashed lines). The synthetic photometry used to fit the model are shown as squares. Each legend shows the disk temperatures, best fit  $\chi^2$ ,  $\lambda_0$ ,  $\beta$ ,  $\mathcal{R}_T$ , and  $\mathcal{R}_f$ .

result of smaller blowout sizes and therefore a wider range of grain temperatures (e.g. Fig. 8).

Fig. 13 shows the temperature and fractional luminosity ratios against stellar temperature for our observed sample (i.e. the same as the top panels of Fig. 6), with the addition of the range of parameters found from the grid of “rocky” composition models in Fig. 12 plotted as red lines. Each vertex corresponds to a model that required a two-temperature blackbody fit. For these grids, vertical solid lines show the effect of varying the size distribution slope  $q$  at constant spectral type, and near-horizontal dashed lines show the effect of varying the spectral type at constant size distribution slope. The trends described above for Fig. 12 are apparent; models with flatter size distributions tends to have lower  $\mathcal{R}_f$ , and  $\mathcal{R}_T$  generally decreases as stellar effective temperature increases but depends only weakly on  $q$ . For this composition, the models have lower  $\mathcal{R}_T$  than most observed disks, and only reproduce the disks with higher  $\mathcal{R}_f$ .

We now introduce the second “icy” composition ( $q_{\text{H}_2\text{O}} = 0.85$ ), plotted as blue lines in Fig. 13. These models have been calculated over the same grid of size distribution slopes and spectral types. A set of SEDs analogous to those in Fig. 12

looks qualitatively similar, and shows the same trends. This icier composition covers a somewhat different range of  $\mathcal{R}_T$  and  $\mathcal{R}_f$ , resulting in two-temperature disks with lower values of both ratios. The effect of changing  $q$  gives a similar change as the difference between the two different compositions in logarithmic  $\mathcal{R}_f$ , suggesting that these can be equally important effects. In general however, flatter size distributions are required to reproduce the lowest observed values of  $\mathcal{R}_f$ . Both models have trouble producing  $\mathcal{R}_T$  as large as those observed, particularly for earlier spectral types due to larger blowout sizes. For the few models where  $\mathcal{R}_T$  is in reasonable agreement,  $\mathcal{R}_f$  is relatively high ( $\gtrsim 1$ ).

To emphasise the  $\mathcal{R}_T$  vs.  $\mathcal{R}_f$  parameter space covered, Fig. 14 shows the model grids compared to our two-temperature sample. As is expected from the variations in Fig. 13, the models do not cover this space in a simple linear fashion, but do show that only disks with relatively low  $\mathcal{R}_T$  are reproduced by narrow belt models. At low  $\mathcal{R}_f$ , model disks with  $\mathcal{R}_T$  larger than about 2 are not seen, increasing to about 3 at higher  $\mathcal{R}_f$ .

As noted above, the main conclusion from Fig. 13 is that  $\mathcal{R}_T$  decreases to more luminous stars; their blowout sizes in-

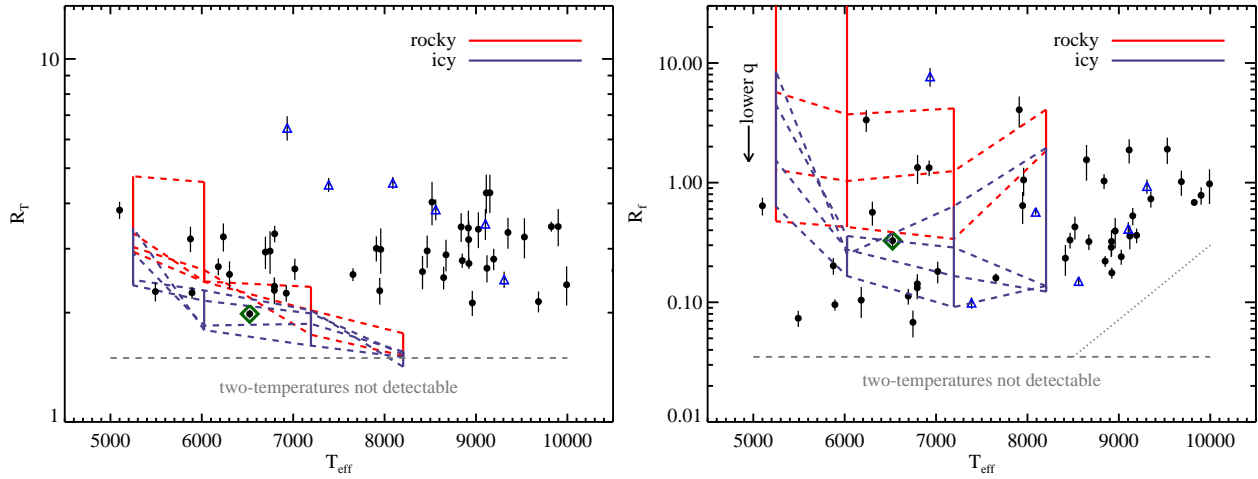


**Figure 13.** Sample of two-temperature debris disks (same as the top panels of Fig. 6), with additional lines showing parameter space covered by the models from size distribution models from Fig. 12 and section 5.2.2. The two different sets of lines show the “rocky” and “icy” compositions we considered. Each vertex represents a model that resulted in a two-temperature disk. Vertical solid lines connect models at constant  $T_{\text{eff}}$  and near-horizontal dashed lines connect models of constant  $q$  (with values of 1.68, 1.72, 1.77, and 1.82 as shown in Fig. 12). The main trends are that earlier spectral types have lower  $\mathcal{R}_T$ , and smaller  $q$  results in lower  $\mathcal{R}_f$ .

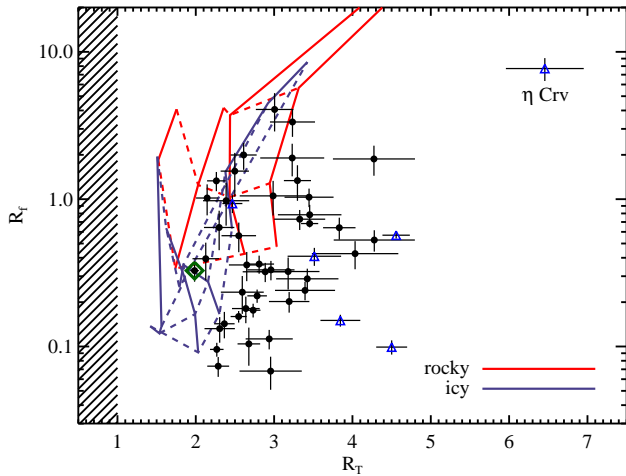


**Figure 14.** Sample of two-temperature debris disks (same as Fig. 4), with lines showing parameter space covered by the models from size distribution models from Fig. 12 and section 5.2.2. The two different sets of lines show the “rocky” and “icy” compositions we considered. Each vertex represents a model that resulted in a two-temperature disk. Solid lines connect models at constant  $T_{\text{eff}}$  and dashed lines connect models of constant  $q$ .

crease with luminosity and they do not show two-temperature spectra for spectral types earlier than about A5. Based on the overlap between the observed two-temperature and model disks in Figs. 13 and 14, Sun-like stars with relatively small  $\mathcal{R}_T$  may be described by our single belt model. The single-belt system HD 181327 lies within our model grids with a range of size distributions depending on the composition ( $q \approx 1.67 - 1.82$ ) compared to the results of Lebreton et al. (2012), who found  $q \approx 1.8$  but used a carefully tuned mix of three material components. That such complex single-belt models can be successfully constructed in individual cases suggests that our two simple models can be taken as a general indication of where plausi-

ble models lie. This parameter space can no doubt be expanded somewhat with more complex prescriptions. We return to tests of this single belt model below.

## 6 DISCUSSION

In the preceding sections, we have shown the properties of a sample of two-temperature debris disks. These disks typically have warm/cool component temperature ratios  $\mathcal{R}_T$  of 2-4, and warm/cool component fractional luminosity ratios  $\mathcal{R}_f$  below ten (Fig. 4). Warm components are detected with  $\mathcal{R}_f$  down to about 0.1, and those fainter than this level become difficult to detect (Fig. 5). Biases in the sample mean that the frequency of the two-temperature phenomenon is hard to estimate, but it appears fairly common, at the tens of percent level.

We then explored how two-temperature disk spectra may arise from narrow planetesimal belts, rather than two distinct belts as is generally assumed. The motivation comes from the known variation of dust temperature with size (Fig. 8), and the possibility that a single belt with properly modelled grain emission might provide a simpler explanation for two-temperature disks than the assumption of multiple belts. We found that a single belt can appear to have two temperatures, but that the specific parameters depend on the size distribution and grain composition assumed. A weakness of this model is that the maximum  $\mathcal{R}_T$  produced is 2-3, smaller than seen for many systems. In addition, the single belt model only works for disks around Sun-like stars, because more luminous stars remove small grains via radiation forces, and the range of grain temperatures across the size distribution is then smaller than observed.

### 6.1 Testing the single belt model

The single belt scenario ultimately relies on the range of temperatures that grains can have at a single stellocentric distance, which range from those of blackbodies at  $T_{\text{BB}}$ , to those of very small grains at  $T_{\text{sm}}$ . To reproduce the low  $\mathcal{R}_f$  values seen for

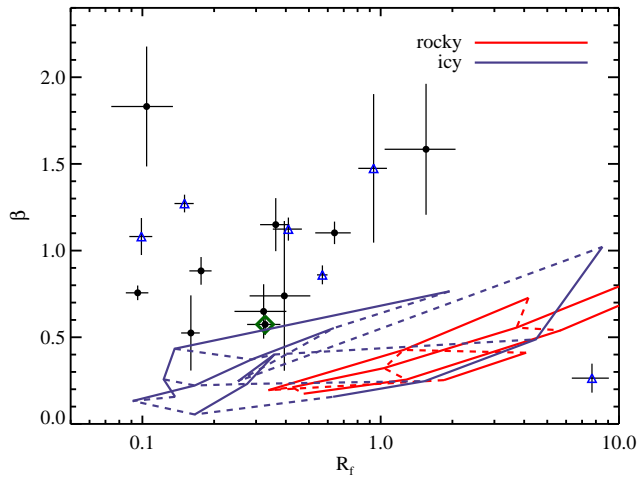


**Figure 15.** Two-temperature debris disks where the far-IR/sub-mm slope  $\beta$  is constrained, with lines showing parameter space covered by the models from size distribution models from Fig. 12 and section 5.2.2. The two different sets of lines show the “rocky” and “icy” compositions we considered. Each vertex represents a model that resulted in a two-temperature disk. Solid lines connect models at constant  $T_{\text{eff}}$  and dashed lines connect models of constant  $q$ . The observed  $\beta$  are generally larger than expected for models with similar  $\mathcal{R}_f$ .

some systems requires relatively flat size distributions, where the two temperature components correspond to these extremes, and in particular the cool component is dominated by emission from objects that behave like blackbodies. A prediction of this scenario is therefore that the true radius of the belt should correspond to that predicted by the blackbody temperature of the cool component, which can be tested in cases where two-temperature disks have been spatially resolved. For example, Morales et al. (2013) found for four two-temperature disks that the resolved size was 2-3 times larger than that predicted by a blackbody. Similar conclusions were reached by Booth et al. (2013) for two resolved disks. Therefore, comparison of predicted and resolved disk sizes does not appear to support the single belt scenario when relatively flat size distributions are required. However, most debris disks are not resolved, so this test is inconclusive in general.

In cases where the cool belts are cool enough for the predicted blackbody size to be in rough agreement with the resolved size, or where the resolved size is unknown, an alternative test can be made. If the cool component is dominated by emission from grains at the blackbody temperature, then the spectral slope of the far-IR and millimetre emission should also appear similar to a blackbody (i.e.  $\beta \approx 0$ ). This property can be seen in Fig. 12, where  $\beta$  is closer to zero for disks with flatter size distributions (left column). In these spectra  $\beta$  does not reach zero because the cool component contains some emission from grains large enough to have near-blackbody temperatures, but small enough to emit inefficiently at sub-mm wavelengths.

To illustrate this point, Figure 15 shows two-temperature disks from our sample where  $\beta$  is constrained, which includes a range of host spectral types. The plot also includes the grids of models described in section 5.2.2. The size distribution slope  $q$  affects both  $\beta$  and  $\mathcal{R}_f$ , so this plot tests whether the  $\beta$  predicted for a given  $\mathcal{R}_f$  is similar to that observed. The models are again shown as lines of constant  $T_{\text{eff}}$  (solid) and  $q$  (dashed),

and as in Fig. 14 the models do not cover this space in a simple linear fashion. Overall however, these models predict lower  $\beta$  for lower  $\mathcal{R}_f$ , and for the compositions used here consistently lie below the observed disks, with the exception of  $\eta$  Crv, which lies below the models. Different or more complex grain models could be consistent with disks that lie near the model lines, with HD 181327 being a specific example. Overall however, the single belt model again appears inconsistent with the observed disk properties in the few cases where it can be tested. This test can only be made for relatively few disks because sufficiently sensitive observations at far-IR/mm wavelengths are required, and these are difficult to obtain. This difficulty leads to a bias, in that disks with lower  $\beta$  are more easily detected at long wavelengths (i.e. those closer to pure blackbodies), and strengthens the conclusion that the observed two-temperature disks have larger  $\beta$  than expected from the single belt model.

Disks that lie close to HD 181327 in Fig. 15 may be the best place to look for two-temperature disks arising from single belts. The four lying along a locus with similar slope to the models are HD 39060 ( $\beta$  Pic), HD 32297, HD 110411 ( $\rho$  Vir), and HD 161868 ( $\gamma$  Oph). Of these,  $\beta$  Pic has a well studied and complex disk structure, that extends over a range of radii (e.g. Smith & Terrile 1984; Telesco et al. 2005; Dent et al. 2014). HD 32297 was modelled as two belts by Donaldson et al. (2013), and while they find that the inner component could not be accounted for by their models of the outer component, this putative inner component has yet to be confirmed. HD 110411 and HD 161868 are have relatively little spatial disk information and no resolved detection of an inner component (Moerchen et al. 2010; Booth et al. 2013). Therefore, three of these four disks represent worthy targets for future high resolution imaging that test for the presence of inner disk components.

In summary, our models show that in some cases two-temperature disks can arise from single belts. As long as the minimum grain size is set by radiation pressure, two-temperature disks around A-type stars probably arise from multiple belts. In addition, a few two-temperature disks have been confirmed to have multiple belts by high resolution observations, and these comprise both A-type and Sun-like stars. For Sun-like stars, single belt models, particularly those with relatively flat size distributions, can produce two temperature disks, and this model is not conclusively ruled out because not all disks are resolved and/or detected at far-IR/mm wavelengths. Where observations exist however, this model is disfavoured. In addition, the flatter size distributions are steeper than those expected from collisional models and inferred from detailed modelling of well characterised systems. Therefore, in general, the assumption that two temperature disks have multiple belts should not be made without considering the properties of those disks and their host stars, but it seems likely that the bulk of two-temperature disks do arise from multiple belts.

## 6.2 Evolution of multiple belts

We now consider whether our results shed light on the origin of multiple belts, which in general appear to be the origin of two-temperature disks. A possible constraint could come from the expected collisional evolution. For example, if two-temperature disks arise from a single belt and the material compositions do not change, no significant evolution of  $\mathcal{R}_f$  or  $\mathcal{R}_T$  would be expected over time because the observed emission always

comes from material in the same location. However, this similarity may also be expected if the warm belts are made of material delivered from the outer belt, perhaps scattered by planets (e.g. Wyatt et al. 2007; Bonsor & Wyatt 2012), in which case the brightness of the inner belt is reasonably connected to that of the outer one.

On the other hand, if two temperatures arise from two independent belts (i.e. as in the Solar system), the two belts are expected to collisionally evolve at different rates. We can estimate the results of differential evolution by assuming that two belts at different radii began their evolution at the same time, soon after the debris disk emerged from the gaseous protoplanetary disk. The collision rate in the disk depends strongly on orbital radius, and for an equal number of objects is higher at smaller radii due both to greater relative velocities and a smaller enclosed volume. The brightness of a belt will start to decay when the largest objects start to collide, which will take longer for the outer belt. Therefore, for two belts that have the same initial brightness, the inner one will start to decay first, and the outer belt will follow later, and all other things being equal, in the long term the brightness difference between two belts is set by the difference in their radii.

Wyatt et al. (2007) estimate that the maximum fractional luminosity of an individual belt is

$$f_{\max} = 1.6 \times 10^{-4} r^{7/3} M_{\star}^{-5/6} L_{\star}^{-0.5} t^{-1}, \quad (10)$$

where the variables are disk radius (in au), stellar mass and luminosity (in Solar units), and system age (in Myr). This fractional luminosity applies to all disks because the brightness decay rate is proportional to the disk mass (and hence the brightness). Thus, all disks tend to the same brightness level once the most massive objects have started to collide. In disks with relatively low initial masses the largest objects take longer to start to collide and decay, and until that time the fractional luminosity lies below the level given by equation (10).

This theory was applied to systems with dust at au scales, such as  $\eta$  Crv and HD 69830 (Wyatt et al. 2007). These disks were found to lie well above  $f_{\max}$  and were deemed “transient”, in that they could not be described by this model of collisional evolution. Here however, the warm dust components lie roughly in the range of a few to 10 au, so for the typical <Gyr ages of objects in our sample the observed fractional luminosities of both the warm and cool components are comparable with  $f_{\max}$ , rather than significantly above it. This agreement suggests that the warm components, if interpreted as distinct belts, are undergoing the collisional evolution expected within the framework of this model, but are not brighter than expected (with the notable exception of  $\eta$  Crv). This inference in turn suggests that we may see the differential evolution of warm/cool component brightnesses described above. However, given the radii inferred for the warm components and their correspondingly long collision timescales, which may be similar to their ages (e.g. Gáspár et al. 2013), the non-detection of such differential evolution would not rule out the two-belt scenario.

To consider the expected evolution of  $\mathcal{R}_f$ , we assume a typical  $\mathcal{R}_T$  of 3, so the radii are a factor of 9 different. Initially, both belts will be very bright, having just emerged from the protoplanetary disk phase, so if both belts are assumed to be near to radially optically thick then  $\mathcal{R}_f$  will be of order unity (but could of course be different, for example if the outer disk is shadowed by the inner one, Kennedy et al. 2014). The brightness of the inner belts is expected to be currently decaying, though this de-

cah may have only begun recently. The outer belts, at roughly ten times greater distances are not expected to be decreasing in brightness significantly due to much longer collision timescales (roughly a factor  $10^4$ ). Therefore, the basic expectation is that the ratio of warm/cool belt brightnesses will start somewhere near unity and decrease over time. Given sufficient time, the difference in belt radii implies this ratio would eventually reach a value of

$$\mathcal{R}_{f,\max} = f_{\max,\text{warm}}/f_{\max,\text{cool}} = \mathcal{R}_T^{-14/3}, \quad (11)$$

or approximately  $10^{-2}$  to  $10^{-3}$ . However, the evolution is sufficiently slow that this limit will not be reached for the  $\lesssim$ Gyr ages within our sample.

Fig. 16 shows the evolution of  $\mathcal{R}_f$  with time for our sample. We use ages from Di Folco et al. (2004); Su et al. (2013); Chen et al. (2014), but adjust the age of the  $\beta$  Pictoris moving group to 20 Myr (Binks & Jeffries 2014), and the age of HD 61005 to 40 Myr (De Silva et al. 2013). These ages are of course very uncertain and there are many disagreements in the literature, but there is a reasonable age distinction between moving group/association stars and older field stars (listed by Chen et al. 2014), so the ages should at least be representative. No significant evolution is seen, though this lack of evolution does not strongly rule out the hypothesis that the two temperatures correspond to two distinct belts. An additional expectation is that the ages of two-temperature systems would be biased towards young ages, because the warm components should decay to undetectable levels more rapidly than the cool components. Our sample is inevitably biased towards younger ages due to young disks being brighter, so any conclusions drawn based on the relative youth of our sample would not be definitive. While Chen et al. (2014) find that two-temperature disks are more likely to be found around younger stars, this tendency is not strong and 50% of their two-temperature disks are  $\gtrsim$ 100 Myr old.

In summary, we cannot rule out the hypothesis that two-temperature disks arise from two independent belts that are decaying due to collisions. The reason being that the warm belts are at sufficiently large radial distances that their brightness is not at odds with models of collisional evolution.

### 6.3 Planetary system structure

Our main conclusion is that most two-temperature debris disks comprise two disk components. Consideration of collisional models shows that these components could be two independent belts undergoing normal collisional evolution, analogous to the Solar System’s Asteroid and Edgeworth-Kuiper belts. The exception among our sample is  $\eta$  Crv, whose warm component is too bright to be explained by collisional models and may originate from material scattered from the outer belt (e.g. Wyatt et al. 2007; Lisse et al. 2012). In other systems the inner components may also be linked to the outer belts via inward scattering of material by intervening planets (e.g. Bonsor & Wyatt 2012). While such a scenario is not required to explain the observed warm dust levels, such scattering no doubt occurs in some, and perhaps all, systems.

Considering the scattering scenario, the inner belt is generally thought to originate due to objects depositing their mass near the star after passing inside some comet sublimation and/or disintegration radius (e.g. Kobayashi et al. 2008;

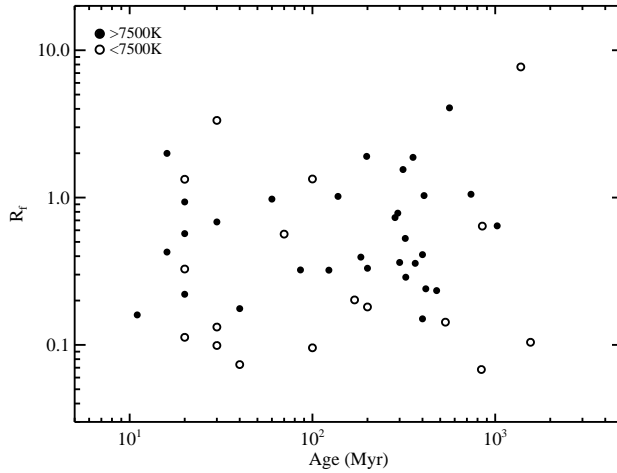


**Figure 16.** Dependence of  $\mathcal{R}_f$  on stellar age. No trends are visible, but the  $\sim 10$  au radii of the warm components and their relatively slow collisional evolution means that the collisional two-belt scenario is not ruled out.

Bonsor & Wyatt 2012; Bonsor et al. 2012). Naively, such a picture is inconsistent with the trend towards higher warm component temperatures for more massive stars, since sublimation should occur at constant temperature. In addition, we find that the warm components can be as cool as 100 K around Sun-like stars, lower than the expected sublimation temperature of  $\sim 150$  K. However, as planetesimals are scattered inward they will collide most often at stellocentric distances near the innermost planet where the volume density and relative velocities are highest, and may even be disrupted due to tidal forces given sufficiently close encounters with this planet. In this case the scattering scenario still allows the creation of two-temperature disks in the absence of thermal destruction of planetesimals within a few au of the star.

Circumstantial evidence that warm and cool belts are separated by planets is provided by extra-Solar systems with two disk components and intervening planets, but does not distinguish between the independent-belt and scattering scenarios. The two belts in the HR 8799 system are separated by a series of massive planets (Marois et al. 2008; Reidemeister et al. 2009; Su et al. 2009; Matthews et al. 2014), and HD 95086 has a single planet that resides in a two-temperature disk (Rameau et al. 2013; Moór et al. 2013), though the warm component has yet to be confirmed by high resolution observations for the latter system.

The  $\sim 10$  au typical radii of the warm components of our two-temperature disks do not rule out planets and debris disks at smaller distances. These tend to be much less massive and much harder to detect (e.g. Howard et al. 2012; Kennedy & Wyatt 2013), so it seems probable that low-mass planets and fainter exo-Zodiacal clouds reside interior to the warm components of the disks we have considered here.

Therefore, in either of the above scenarios, two-temperature debris disks seem to give information on the typical scales of outer planetary systems, with the warm/cool temperature ratios suggesting that these typically span a factor of ten in radius.

## 7 CONCLUSIONS

We have presented a study of debris disks whose emission spectra are well modelled by dust at two temperatures. These disks are typically assumed to be a sign of multiple belts, so here our goal was to explore whether this emission could arise from dust in a single belt, with the range of temperatures arising from the natural variation in grain temperature with size.

We collected a sample of 48 nearby stars with two-temperature debris disks, and used the ratios of warm/cool component temperatures ( $\mathcal{R}_T$ ) and fractional luminosities ( $\mathcal{R}_f$ ) as a diagnostic of disk properties. A plot of  $\mathcal{R}_f$  versus  $\mathcal{R}_T$  shows that  $\eta$  Crv is clearly an outlier among two-temperature disks, having an unusually large warm/cool temperature ratio. We also identified HD 145689 as a potentially interesting system, where the M9 companion may orbit outside or between two debris disk components, or host a disk itself.

Using a grain emission model, we test whether two-temperature disks can arise from single belts. As long as the minimum grain size is set by radiation pressure, two-temperature disks around A-type stars probably arise from multiple belts. In addition, a few two-temperature disks have been confirmed to have multiple belts by high resolution observations, and these comprise both A-type and Sun-like stars. For Sun-like stars, our single-belt model can produce two temperature disks. Where observations allow tests to be made this model is disfavoured, but it is not conclusively ruled out because not all disks are resolved and/or detected at far-IR/mm wavelengths. In general therefore, the assumption that two temperature disks have multiple belts should not be made, but it seems likely that the bulk of two-temperature disks do arise from multiple belts. As noted at the outset, PR drag may allow disks whose planetesimals reside in a narrow belt to have two temperatures due to small grains extending in towards the star. Whether this process can generically reproduce a subset of two-temperature disks is clearly worth future effort.

Assuming the multiple belt interpretation is correct, we considered the expected collisional evolution of two distinct belts. Aside from  $\eta$  Crv, the warm components could be independent belts undergoing normal collisional evolution, so it is possible that two-temperature disks represent systems with analogues of the Asteroid and Edgeworth-Kuiper belts that are separated by planets. Scattering of material from the outer regions could still be an important, or even dominant, mechanism for creating two-temperature debris disks, with the warm component comprising material scattered from the cool component, again due to the presence of intervening planets. For either scenario, the ratio of warm/cool component temperatures is indicative of the scale of outer planetary systems, which typically span a factor of about ten in radius.

## ACKNOWLEDGEMENTS

This work was supported by the European Union through ERC grant number 279973. We thank the referee for their comments and suggestions, Alexander Krivov for helpful discussions, and Christine Chen and Kate Su for sharing their IRS spectra.

## REFERENCES

Acke, B. et al. 2012, *A&A*, 540, A125



- Augereau, J. C., Lagrange, A. M., Mouillet, D., Papaloizou, J. C. B., & Grorod, P. A. 1999, *A&A*, 348, 557
- Aumann, H. H., Beichman, C. A., Gillett, F. C., de Jong, T., Houck, J. R., Low, F. J., Neugebauer, G., Walker, R. G., & Wesselsius, P. R. 1984, *ApJ*, 278, L23
- Backman, D., Marengo, M., Stapelfeldt, K., Su, K., Wilner, D., Dowell, C. D., Watson, D., Stansberry, J., Rieke, G., Megeath, T., Fazio, G., & Werner, M. 2009, *ApJ*, 690, 1522
- Ballering, N. P., Rieke, G. H., Su, K. Y. L., & Montiel, E. 2013, *ApJ*, 775, 55
- Beichman, C. A. et al. 2006, *ApJ*, 652, 1674
- Binks, A. S. & Jeffries, R. D. 2014, *MNRAS*, 438, L11
- Bonsor, A., Augereau, J.-C., & Thébault, P. 2012, *A&A*, 548, A104
- Bonsor, A. & Wyatt, M. C. 2012, *MNRAS*, 420, 2990
- Booth, M. et al. 2013, *MNRAS*, 428, 1263
- Brott, I. & Hauschildt, P. H. 2005, in *ESA Special Publication*, Vol. 576, *The Three-Dimensional Universe with Gaia*, ed. C. Turon, K. S. O’Flaherty, & M. A. C. Perryman, 565
- Bryden, G., Beichman, C. A., Carpenter, J. M., Rieke, G. H., Stapelfeldt, K. R., Werner, M. W., Tanner, A. M., Lawler, S. M., Wyatt, M. C., Trilling, D. E., Su, K. Y. L., Blaylock, M., & Stansberry, J. A. 2009, *ApJ*, 705, 1226
- Burns, J. A., Lamy, P. L., & Soter, S. 1979, *Icarus*, 40, 1
- Carpenter, J. M., Bouwman, J., Silverstone, M. D., Kim, J. S., Stauffer, J., Cohen, M., Hines, D. C., Meyer, M. R., & Crockett, N. 2008, *ApJS*, 179, 423
- Carpenter, J. M., Wolf, S., Schreyer, K., Launhardt, R., & Henning, T. 2005, *AJ*, 129, 1049
- Castelli, F. & Kurucz, R. L. 2003, in *IAU Symposium*, Vol. 210, *Modelling of Stellar Atmospheres*, ed. N. Piskunov, W. W. Weiss, & D. F. Gray, 20P
- Chen, C. H., Li, A., Bohac, C., Kim, K. H., Watson, D. M., van Cleve, J., Houck, J., Stapelfeldt, K., Werner, M. W., Rieke, G., Su, K., Marengo, M., Backman, D., Beichman, C., & Fazio, G. 2007, *ApJ*, 666, 466
- Chen, C. H., Mittal, T., Kuchner, M., Forrest, W. J., Lisse, C. M., Manoj, P., Sargent, B. A., & Watson, D. M. 2014, *ApJS*, 211, 25
- Chen, C. H., Sargent, B. A., Bohac, C., Kim, K. H., Leibensperger, E., Jura, M., Najita, J., Forrest, W. J., Watson, D. M., Sloan, G. C., & Keller, L. D. 2006, *ApJS*, 166, 351
- Chen, C. H., Sheehan, P., Watson, D. M., Manoj, P., & Najita, J. R. 2009, *ApJ*, 701, 1367
- Chini, R., Kruegel, E., Kreysa, E., Shustov, B., & Tutukov, A. 1991, *A&A*, 252, 220
- Churcher, L., Wyatt, M., & Smith, R. 2011, *MNRAS*, 410, 2
- Cutri, R. M. et al. 2003, *2MASS All Sky Catalog of point sources*.
- De Silva, G. M., D’Orazi, V., Melo, C., Torres, C. A. O., Gieles, M., Quast, G. R., & Sterzik, M. 2013, *MNRAS*, 431, 1005
- Dent, W. R. F., Wyatt, M. C., Roberge, A., Augereau, J.-C., Casassus, S., Corder, S., Greaves, J. S., de Gregorio-Monsalvo, I., Hales, A., Jackson, A. P., Hughes, A. M., Lagrange, A.-M., Matthews, B., & Wilner, D. 2014, *ArXiv e-prints*
- Di Folco, E., Thévenin, F., Kervella, P., Domiciano de Souza, A., Coudé du Foresto, V., Ségransan, D., & Morel, P. 2004, *A&A*, 426, 601
- Dohnanyi, J. S. 1969, *J. Geophys. Res.*, 74, 2531
- Donaldson, J. K., Lebreton, J., Roberge, A., Augereau, J.-C., & Krivov, A. V. 2013, *ApJ*, 772, 17
- Duchêne, G., Arriaga, P., Wyatt, M., Kennedy, G., Sibthorpe, B., Lisse, C., Holland, W., Wisniewski, J., Clampin, M., Kalas, P., Pinte, C., Wilner, D., Booth, M., Horner, J., Matthews, B., & Greaves, J. 2014, *ApJ*, 784, 148
- Eiroa, C. et al. 2013, *A&A*, 555, A11
- Foreman-Mackey, D., Hogg, D. W., Lang, D., & Goodman, J. 2012, *ArXiv e-prints*
- Gáspár, A., Psaltis, D., Rieke, G. H., & Özel, F. 2012, *ApJ*, 754, 74
- Gáspár, A., Rieke, G. H., & Balog, Z. 2013, *ApJ*, 768, 25
- Goodman, J. & Weare, J. 2010, *Comm. App. Math. Comp. Sci.*, 5, 65
- Greaves, J. S., Holland, W. S., Wyatt, M. C., Dent, W. R. F., Robson, E. I., Coulson, I. M., Jenness, T., Moriarty-Schieven, G. H., Davis, G. R., Butner, H. M., Gear, W. K., Dominik, C., & Walker, H. J. 2005, *ApJ*, 619, L187
- Helou, G. 1989, in *IAU Symposium*, Vol. 135, *Interstellar Dust*, ed. L. J. Allamandola & A. G. G. M. Tielens, 285
- Helou, G. & Walker, D. W., eds. 1988, *Infrared astronomical satellite (IRAS) catalogs and atlases. Volume 7: The small scale structure catalog*, Vol. 7
- Høg, E., Fabricius, C., Makarov, V. V., Urban, S., Corbin, T., Wycoff, G., Bastian, U., Schwekendiek, P., & Wicencec, A. 2000, *A&A*, 355, L27
- Holland, W. S., Greaves, J. S., Dent, W. R. F., Wyatt, M. C., Zuckerman, B., Webb, R. A., McCarthy, C., Coulson, I. M., Robson, E. I., & Gear, W. K. 2003, *ApJ*, 582, 1141
- Holland, W. S., Greaves, J. S., Zuckerman, B., Webb, R. A., McCarthy, C., Coulson, I. M., Walther, D. M., Dent, W. R. F., Gear, W. K., & Robson, I. 1998, *Nature*, 392, 788
- Holmes, E. K., Butner, H. M., Fajardo-Acosta, S. B., & Rebull, L. M. 2003, *AJ*, 125, 3334
- Houck, J. R. et al. 2004, *ApJS*, 154, 18
- Howard, A. W. et al. 2012, *ApJS*, 201, 15
- Huélamo, N., Nürnberger, D. E. A., Ivanov, V. D., Chauvin, G., Carraro, G., Sterzik, M. F., Melo, C. H. F., Bonnefoy, M., Hartung, M., Haubois, X., & Foellmi, C. 2010, *A&A*, 521, L54
- Hughes, A. M., Wilner, D. J., Andrews, S. M., Williams, J. P., Su, K. Y. L., Murray-Clay, R. A., & Qi, C. 2011, *ApJ*, 740, 38
- Ishihara, D. et al. 2010, *A&A*, 514, A1
- Kalas, P., Graham, J. R., & Clampin, M. 2005, *Nature*, 435, 1067
- Kennedy, G. M., Murphy, S. J., Lisse, C. M., Ménard, F., Sitko, M. L., Wyatt, M. C., Bayliss, D. D. R., DeMeo, F. E., Crawford, K. B., Kim, D. L., Rudy, R. J., Russell, R. W., Sibthorpe, B., Skinner, M. A., & Zhou, G. 2014, *MNRAS*
- Kennedy, G. M. & Wyatt, M. C. 2013, *MNRAS*, 433, 2334
- Kennedy, G. M., Wyatt, M. C., Sibthorpe, B., Phillips, N. M., Matthews, B. C., & Greaves, J. S. 2012, *MNRAS*, 426, 2115
- Kobayashi, H., Watanabe, S.-i., Kimura, H., & Yamamoto, T. 2008, *Icarus*, 195, 871
- Krist, J. E., Stapelfeldt, K. R., Bryden, G., Rieke, G. H., Su, K. Y. L., Chen, C. C., Beichman, C. A., Hines, D. C., Rebull, L. M., Tanner, A., Trilling, D. E., Clampin, M., & Gáspár, A. 2010, *AJ*, 140, 1051
- Laor, A. & Draine, B. T. 1993, *ApJ*, 402, 441
- Lawler, S. M., Beichman, C. A., Bryden, G., Ciardi, D. R., Tanner, A. M., Su, K. Y. L., Stapelfeldt, K. R., Lisse, C. M.,

- & Harker, D. E. 2009, *ApJ*, 705, 89
- Lebouteiller, V., Barry, D. J., Spoon, H. W. W., Bernard-Salas, J., Sloan, G. C., Houck, J. R., & Weedman, D. W. 2011, *ApJS*, 196, 8
- Lebreton, J., Augereau, J.-C., Thi, W.-F., Roberge, A., Donaldson, J., Schneider, G., Maddison, S. T., Ménard, F., Riviere-Marichalar, P., Mathews, G. S., Kamp, I., Pinte, C., Dent, W. R. F., Barrado, D., Duchêne, G., Gonzalez, J.-F., Grady, C. A., Meeus, G., Pantin, E., Williams, J. P., & Woitke, P. 2012, *A&A*, 539, A17
- Li, A. & Greenberg, J. M. 1997, *A&A*, 323, 566
- , 1998, *A&A*, 331, 291
- Liseau, R., Brandeker, A., Fridlund, M., Olofsson, G., Takeuchi, T., & Artymowicz, P. 2003, *A&A*, 402, 183
- Liseau, R. et al. 2010, *A&A*, 518, L132
- Lisse, C. M., Wyatt, M. C., Chen, C. H., Morlok, A., Watson, D. M., Manoj, P., Sheehan, P., Currie, T. M., Thebault, P., & Sitko, M. L. 2012, *ApJ*, 747, 93
- Löhne, T. et al. 2012, *A&A*, 537, A110
- Maness, H. L., Fitzgerald, M. P., Paladini, R., Kalas, P., Duchene, G., & Graham, J. R. 2008, *ApJ*, 686, L25
- Marois, C., Macintosh, B., Barman, T., Zuckerman, B., Song, I., Patience, J., Lafrenière, D., & Doyon, R. 2008, *Science*, 322, 1348
- Matthews, B. et al. 2014, *ApJ*, 780, 97
- Matthews, B. C., Kalas, P. G., & Wyatt, M. C. 2007, *ApJ*, 663, 1103
- Moerchen, M. M., Telesco, C. M., & Packham, C. 2010, *ApJ*, 723, 1418
- Moerchen, M. M., Telesco, C. M., Packham, C., & Kehoe, T. J. 2007, *ApJ*, 655, L109
- Moór, A., Ábrahám, P., Kóspál, Á., Szabó, G. M., Apai, D., Balog, Z., Csengeri, T., Grady, C., Henning, T., Juhász, A., Kiss, C., Pascucci, I., Szulágyi, J., & Vavrek, R. 2013, *ApJ*, 775, L51
- Moór, A., Pascucci, I., Kóspál, Á., Ábrahám, P., Csengeri, T., Kiss, L. L., Apai, D., Grady, C., Henning, T., Kiss, C., Bayliss, D., Juhász, A., Kovács, J., & Szalai, T. 2011, *ApJS*, 193, 4
- Morales, F. Y., Bryden, G., Werner, M. W., & Stapelfeldt, K. R. 2013, *ApJ*, 776, 111
- Morales, F. Y., Rieke, G. H., Werner, M. W., Bryden, G., Stapelfeldt, K. R., & Su, K. Y. L. 2011, *ApJ*, 730, L29
- Morales, F. Y., Werner, M. W., Bryden, G., Plavchan, P., Stapelfeldt, K. R., Rieke, G. H., Su, K. Y. L., Beichman, C. A., Chen, C. H., Grogan, K., Kenyon, S. J., Moro-Martin, A., & Wolf, S. 2009, *ApJ*, 699, 1067
- Moshir, M. et al. 1990, in *IRAS Faint Source Catalogue*, version 2.0 (1990), 0
- Najita, J. & Williams, J. P. 2005, *ApJ*, 635, 625
- Nesvorný, D., Jenniskens, P., Levison, H. F., Bottke, W. F., Vokrouhlický, D., & Gounelle, M. 2010, *ApJ*, 713, 816
- Nilsson, R., Liseau, R., Brandeker, A., Olofsson, G., Pilbratt, G. L., Risacher, C., Rodmann, J., Augereau, J.-C., Bergman, P., Eiroa, C., Fridlund, M., Thébault, P., & White, G. J. 2010, *A&A*, 518, A40
- Nilsson, R., Liseau, R., Brandeker, A., Olofsson, G., Risacher, C., Fridlund, M., & Pilbratt, G. 2009, *A&A*, 508, 1057
- O'Brien, D. P. & Greenberg, R. 2003, *Icarus*, 164, 334
- Olofsson, J., Henning, T., Nielbock, M., Augereau, J.-C., Juhász, A., Oliveira, I., Absil, O., & Tamanai, A. 2013, *A&A*, 551, A134
- Perryman, M. A. C. & ESA, eds. 1997, *ESA Special Publication*, Vol. 1200, *The HIPPARCOS and TYCHO catalogues. Astrometric and photometric star catalogues derived from the ESA HIPPARCOS Space Astrometry Mission*
- Phillips, N. M. 2011, PhD thesis, The University of Edinburgh
- Phillips, N. M., Greaves, J. S., Dent, W. R. F., Matthews, B. C., Holland, W. S., Wyatt, M. C., & Sibthorpe, B. 2010, *MNRAS*, 403, 1089
- Rameau, J., Chauvin, G., Lagrange, A.-M., Meshkat, T., Boccaletti, A., Quanz, S. P., Currie, T., Mawet, D., Girard, J. H., Bonnefoy, M., & Kenworthy, M. 2013, *ApJ*, 779, L26
- Rebull, L. M. et al. 2008, *ApJ*, 681, 1484
- Reidemeister, M., Krivov, A. V., Schmidt, T. O. B., Fiedler, S., Müller, S., Löhne, T., & Neuhäuser, R. 2009, *A&A*, 503, 247
- Reidemeister, M., Krivov, A. V., Stark, C. C., Augereau, J.-C., Löhne, T., & Müller, S. 2011, *A&A*, 527, A57
- Rieke, G. H., Blaylock, M., Decin, L., Engelbracht, C., Ogle, P., Avrett, E., Carpenter, J., Cutri, R. M., Armus, L., Gordon, K., Gray, R. O., Hinz, J., Su, K., & Willmer, C. N. A. 2008, *AJ*, 135, 2245
- Rieke, G. H. et al. 2004, *ApJS*, 154, 25
- Roberge, A. et al. 2012, *PASP*, 124, 799
- Roccatagliata, V., Henning, T., Wolf, S., Rodmann, J., Corder, S., Carpenter, J. M., Meyer, M. R., & Dowell, D. 2009, *A&A*, 497, 409
- Rodriguez, D. R. & Zuckerman, B. 2012, *ApJ*, 745, 147
- Schneider, G., Silverstone, M. D., Hines, D. C., Augereau, J.-C., Pinte, C., Ménard, F., Krist, J., Clampin, M., Grady, C., Golimowski, D., Ardila, D., Henning, T., Wolf, S., & Rodmann, J. 2006, *ApJ*, 650, 414
- Schüppler, C., Löhne, T., Krivov, A. V., Ertel, S., Marshall, J. P., & Eiroa, C. 2014, *ArXiv e-prints*
- Sheret, I., Dent, W. R. F., & Wyatt, M. C. 2004, *MNRAS*, 348, 1282
- Sibthorpe, B. et al. 2010, *A&A*, 518, L130
- Smith, B. A. & Terrile, R. J. 1984, *Science*, 226, 1421
- Smith, R., Churcher, L. J., Wyatt, M. C., Moerchen, M. M., & Telesco, C. M. 2009a, *A&A*, 493, 299
- Smith, R., Wyatt, M. C., & Haniff, C. A. 2009b, *A&A*, 503, 265
- Su, K. Y. L., Rieke, G. H., Stansberry, J. A., Bryden, G., Stapelfeldt, K. R., Trilling, D. E., Muzerolle, J., Beichman, C. A., Moro-Martin, A., Hines, D. C., & Werner, M. W. 2006, *ApJ*, 653, 675
- Su, K. Y. L., Rieke, G. H., Stapelfeldt, K. R., Malhotra, R., Bryden, G., Smith, P. S., Misselt, K. A., Moro-Martin, A., & Williams, J. P. 2009, *ApJ*, 705, 314
- Su, K. Y. L. et al. 2013, *ApJ*, 763, 118
- Sylvester, R. J., Skinner, C. J., Barlow, M. J., & Mannings, V. 1996, *MNRAS*, 279, 915
- Telesco, C. M., Fisher, R. S., Wyatt, M. C., Dermott, S. F., Kehoe, T. J. J., Novotny, S., Mariñas, N., Radomski, J. T., Packham, C., De Buizer, J., & Hayward, T. L. 2005, *Nature*, 433, 133
- van Leeuwen, F. 2007, *A&A*, 474, 653
- van Lieshout, R., Dominik, C., Kama, M., & Min, M. 2014, *ArXiv e-prints*
- Vandenbussche, B. et al. 2010, *A&A*, 518, L133
- Wahhaj, Z., Koerner, D. W., Backman, D. E., Werner, M. W., Serabyn, E., Ressler, M. E., & Lis, D. C. 2005, *ApJ*, 618, 385
- Walker, H. J. & Butner, H. M. 1995, *Ap&SS*, 224, 389
- Werner, M. W. et al. 2004, *ApJS*, 154, 1

- Williams, J. P. & Andrews, S. M. 2006, *ApJ*, 653, 1480
- Williams, J. P., Najita, J., Liu, M. C., Bottinelli, S., Carpenter, J. M., Hillenbrand, L. A., Meyer, M. R., & Soderblom, D. R. 2004, *ApJ*, 604, 414
- Wilner, D. J., Holman, M. J., Kuchner, M. J., & Ho, P. T. P. 2002, *ApJ*, 569, L115
- Wright, E. L. et al. 2010, *AJ*, 140, 1868
- Wyatt, M. C. 2005, *A&A*, 433, 1007
- Wyatt, M. C. & Dent, W. R. F. 2002, *MNRAS*, 334, 589
- Wyatt, M. C., Greaves, J. S., Dent, W. R. F., & Coulson, I. M. 2005, *ApJ*, 620, 492
- Wyatt, M. C., Smith, R., Greaves, J. S., Beichman, C. A., Bryden, G., & Lisse, C. M. 2007, *ApJ*, 658, 569
- Wyatt, M. C. et al. 2012, *MNRAS*, 424, 1206
- Zuckerman, B., Rhee, J. H., Song, I., & Bessell, M. S. 2011, *ApJ*, 732, 61

**APPENDIX A: SAMPLE AND (SUB-)MM  
PHOTOMETRY**

**Table A1.** Sample and results of blackbody fitting for 48 two-temperature disks, 9 sources marked with a \* are part of the DEBRIS sample (Phillips et al. 2010). The “Ref” column notes papers from which far-IR photometry was obtained: 1: Helou & Walker (1988), 2: Moshir et al. (1990), 3: Su et al. (2006), 4: Rebull et al. (2008), 5: Carpenter et al. (2008), 6: Bryden et al. (2009), 7: Morales et al. (2009), 8: Su et al. (2009), 9: Sibthorpe et al. (2010), 10: Liseau et al. (2010), 11: Vandenbussche et al. (2010), 12: Zuckerman et al. (2011), 13: Moór et al. (2011), 14: Phillips (2011), 15: Acke et al. (2012), 16: Gáspár et al. (2013), 17: Booth et al. (2013).

Name	$T_*$	Age (Myr)	$T_{\text{warm}}$	$e_{T_{\text{warm}}}$	$T_{\text{cool}}$	$e_{T_{\text{cool}}}$	$\lambda_0$	$e_{\lambda_0}$	$\beta$	$e_{\beta}$	$\mathcal{R}_T$	$e_{\mathcal{R}_T}$	$\mathcal{R}_f$	$e_{\mathcal{R}_f}$	Ref
HD 377	5876	170	113	9	35	2					3.2	0.3	0.20	0.03	5
HD 6798	9120	365	180	16	68	5					2.7	0.2	0.36	0.08	2
HD 9672	8923	40	143	5	52	2	61	10	0.9	0.1	2.7	0.1	0.18	0.02	2
HD 10647*	6181	1560	99	6	37	2	56	8	1.8	0.3	2.7	0.1	0.10	0.03	2,6,10,16
HD 10939	9026	417	200	23	59	2					3.4	0.4	0.24	0.03	1,7
HD 13246	6236	30	231	22	72	9					3.2	0.3	3.34	0.69	12
HD 14055*	9197	300	183	13	65	2	192	21	1.1	0.2	2.8	0.2	0.36	0.05	2,3,14
HD 15115	6696	20	163	17	55	2					2.9	0.3	0.11	0.02	2,13
HD 15745	6924	20	104	6	46	3					2.3	0.1	1.33	0.20	2,13
HD 16743	7018	200	127	9	48	3					2.6	0.2	0.18	0.04	13
HD 22049*	5100	850	119	7	31	1	73	11	1.1	0.1	3.8	0.2	0.64	0.11	2,6
HD 23267	9992	60	330	42	138	11					2.4	0.3	0.98	0.32	7
HD 25457	6303	70	138	13	54	5					2.5	0.2	0.56	0.13	2,5
HD 30447	6794	30	133	11	58	2					2.3	0.2	0.13	0.03	2,13
HD 31295	8673	123	168	17	58	3					2.9	0.3	0.32	0.05	2,3,14
HD 32297	7654	11	203	9	80	2	237	105	0.5	0.2	2.5	0.1	0.16	0.01	1
HD 38056	9900	293	302	36	88	4					3.5	0.4	0.78	0.13	7
HD 38206	9825	30	233	8	68	2					3.5	0.1	0.68	0.04	2,7
HD 38207	6795	534	123	7	52	2					2.4	0.1	0.14	0.03	5
HD 39060*	8090	20	493	19	108	1	204	15	0.9	0.1	4.6	0.2	0.57	0.03	2,11,14
HD 61005	5492	40	123	8	54	1					2.3	0.1	0.07	0.01	1,5
HD 70313	8466	200	183	19	62	3					3.0	0.3	0.33	0.05	2,7
HD 71722	8917	324	256	30	75	2					3.4	0.4	0.29	0.05	7
HD 79108	9350	283	230	23	69	5					3.3	0.3	0.73	0.11	2,7
HD 80950	9684	138	294	21	137	7					2.1	0.1	1.02	0.24	7
HD 98673	7958	737	244	36	82	7					3.0	0.4	1.05	0.28	7
HD 107146	5893	100	103	4	45	1	338	20	0.8	0.0	2.3	0.1	0.10	0.01	2,5
HD 109085*	6934	1380	254	20	39	2	34	12	0.3	0.1	6.5	0.5	7.70	1.36	2
HD 110411*	8920	86	253	32	79	2	75	9	0.6	0.2	3.2	0.4	0.32	0.08	2,14,17
HD 125162*	8646	313	106	8	42	4	93	24	1.6	0.4	2.5	0.2	1.55	0.51	2,14
HD 136246	8519	16	211	29	52	6					4.0	0.6	0.43	0.09	7
HD 136482	10521	16	296	20	113	8					2.6	0.2	1.99	0.41	7
HD 138965	8850	20	154	7	55	2					2.8	0.1	0.22	0.02	1,7
HD 141378	8415	478	146	16	56	4					2.6	0.3	0.23	0.07	2,7
HD 153053	7947	1025	107	11	46	5					2.3	0.2	0.64	0.19	1,7
HD 159492	7910	562	166	14	55	5					3.0	0.2	4.06	1.18	2,14
HD 161868	8960	184	141	12	66	4	162	95	0.7	0.4	2.1	0.2	0.39	0.11	2,3,14
HD 172167*	9103	400	166	16	47	2	67	5	1.1	0.1	3.5	0.3	0.41	0.06	2,9,14
HD 181296	9308	20	254	14	103	4	87	13	1.5	0.4	2.5	0.1	0.93	0.13	2,4
HD 181327	6524	20	107	3	54	2	59	4	0.6	0.1	2.0	0.1	0.33	0.05	2
HD 182919	9530	198	329	43	102	10					3.2	0.4	1.90	0.47	7
HD 191174	9113	355	330	41	77	6					4.3	0.5	1.87	0.43	7
HD 192425	8838	408	222	21	65	5					3.4	0.3	1.03	0.15	2,7
HD 205674	6747	840	149	20	50	2					3.0	0.4	0.07	0.02	2,13
HD 216956*	8560	400	148	10	39	1	74	6	1.3	0.1	3.8	0.3	0.15	0.01	2,14,15
HD 218396	7388	30	163	7	36	1	67	7	1.1	0.1	4.5	0.2	0.10	0.01	8
HD 221853	6797	100	91	5	28	1					3.3	0.2	1.34	0.36	2,13
HD 225200	9152	322	263	32	61	2					4.3	0.5	0.53	0.09	7

**Table A2.** Sub-mm and mm photometry of targets in our sample. The  $3\sigma$  limit column indicates that the flux is an upper limit. Fluxes without this flag are not necessarily significant detections.

Name	$\lambda(\mu\text{m})$	Instrument	Flux (mJy)	Unc (mJy)	$3\sigma$ flag	Reference
HD 377	3000	OVRO	0.79	0.61		Carpenter et al. (2005)
HD 377	1200	IRAM	4	1		Roccatagliata et al. (2009)
HD 377	2700	OVRO	0.32	0.8		Carpenter et al. (2005)
HD 9672	1300	IRAM	13.9	2.48		Walker & Butner (1995)
HD 14055	850	SCUBA	5.5	1.8		Williams & Andrews (2006)
HD 15115	850	SCUBA	4.9	1.6		Williams & Andrews (2006)
HD 15115	870	LABOCA	15.3		1	Nilsson et al. (2009)
HD 22049	1300	IRAM	12.7	3.9		Walker & Butner (1995)
HD 22049	1300	MPIfR	24.2	3.4		Chini et al. (1991)
HD 22049	450	SCUBA	225	10		Sheret et al. (2004)
HD 22049	850	SCUBA	37	3		Greaves et al. (2005)
HD 22049	450	SCUBA	250	20		Greaves et al. (2005)
HD 22049	350	CSO	366	50		Backman et al. (2009)
HD 22049	850	SCUBA	40	1.5		Sheret et al. (2004)
HD 25457	1200	SEST	-8	14		Carpenter et al. (2005)
HD 25457	870	LABOCA	9.9		1	Nilsson et al. (2010)
HD 25457	2700	OVRO	-1.51	1.33		Carpenter et al. (2005)
HD 25457	3000	OVRO	0.37	0.62		Carpenter et al. (2005)
HD 25457	1200	IRAM	2.2		1	Roccatagliata et al. (2009)
HD 30447	870	LABOCA	6.9	5		Nilsson et al. (2010)
HD 32297	870	LABOCA	19.5		1	Nilsson et al. (2010)
HD 32297	1300	CARMA	5.1	1.1		Maness et al. (2008)
HD 38207	1200	SEST	-3	12		Carpenter et al. (2005)
HD 38207	1200	IRAM	0.33		1	Roccatagliata et al. (2009)
HD 39060	1200	SIMBA	24.3	3		Liseau et al. (2003)
HD 39060	870	LABOCA	63.6	6.7		Nilsson et al. (2009)
HD 39060	850	SCUBA	58.3	6.5		Holland et al. (1998)
HD 39060	1300	MPIfR	24.9	2.6		Chini et al. (1991)
HD 61005	870	LABOCA	18		1	Nilsson et al. (2010)
HD 61005	1200	SEST	31	34		Carpenter et al. (2005)
HD 61005	350	CSO	95	12		Roccatagliata et al. (2009)
HD 107146	350	CSO	319	6		Roccatagliata et al. (2009)
HD 107146	3000	OVRO	1.42	0.23		Carpenter et al. (2005)
HD 107146	850	SCUBA	20	3.2		Najita & Williams (2005)
HD 107146	880	SMA	36	1		Hughes et al. (2011)
HD 107146	450	SCUBA	130	40		Williams et al. (2004)
HD 107146	450	SCUBA	130	12		Najita & Williams (2005)
HD 107146	850	SCUBA	20	4		Williams et al. (2004)
HD 109085	450	SCUBA	58.2	9.8		Wyatt et al. (2005)
HD 109085	850	SCUBA2	15.5	1.4		Duchêne et al. (2014)
HD 109085	850	SCUBA	14.3	1.8		Wyatt et al. (2005)
HD 161868	870	LABOCA	12.8	5.2		Nilsson et al. (2010)
HD 172167	850	SCUBA	45.7	5.4		Holland et al. (1998)
HD 172167	1300	IRAM	11.4	1.7		Wilner et al. (2002)
HD 172167	3300	IRAM	0.39		1	Wilner et al. (2002)
HD 181296	870	LABOCA	14.4		1	Nilsson et al. (2009)
HD 181327	870	LABOCA	51.7	6.2		Nilsson et al. (2009)
HD 181327	3190	ATCA	0.72	0.25		Lebreton et al. (2012)
HD 192425	1300	SMTO	7.95		1	Holmes et al. (2003)
HD 192425	870	SMTO	33.3		1	Holmes et al. (2003)
HD 216956	450	SCUBA	595	35		Holland et al. (2003)
HD 216956	1300	MPIfR	21	2.5		Chini et al. (1991)
HD 216956	850	SCUBA	81	7.2		Holland et al. (1998)
HD 216956	850	SCUBA	97	5		Holland et al. (2003)
HD 218396	850	SCUBA	10.3	1.8		Williams & Andrews (2006)
HD 218396	1100	UKT14	33		1	Sylvester et al. (1996)

The following pages contain flux density distributions (SEDs) for the 48-star sample. Stars are ordered as in Table A1 left to right and down. Each panel is labelled by the stars' HD identifier. Symbols are as in Fig. 1 in the main article.

